Paleoceanography and Paleoclimatology

AGU ADVANCING EARTH AND SPACE SCIENCES

RESEARCH ARTICLE
10.1029/2023PA004809

North Atlantic Temperature Change Across the Eocene-Oligocene Transition From Clumped Isotopes

Ilja J. Kocken[1,2], Peter D. Nooteboom[3], Kasper van der Veen[2], Helen K. Coxall[4], Inigo A. Müller[2,5], A. Nele Meckler[6], and Martin Ziegler[2]

[1]School of Ocean and Earth Science and Techonology, University of Hawai'i at Mānoa, Honolulu, HI, USA, [2]Department of Earth Sciences, Faculty of Geosciences, Utrecht University, Utrecht, The Netherlands, [3]Department of Physics, Faculty of Science, Institute for Marine and Atmospheric Research Utrecht (IMAU), Utrecht University, Utrecht, The Netherlands, [4]Department of Geological Sciences, Stockholm University, Stockholm, Sweden, [5]Section of Earth and Environmental Science, Faculty of Science, University of Geneva, Geneva, Switzerland, [6]Department of Earth Science, Bjerknes Centre for Climate Research, University of Bergen, Bergen, Norway

Abstract The Eocene-Oligocene transition (EOT) (~34 Ma) is marked by the rapid development of a semi-permanent Antarctic ice-sheet, as indicated by ice-rafted debris and a 1–1.5‰ increase in deep sea $\delta^{18}O$. Proxy reconstructions indicate a drop in atmospheric CO_2 and global cooling. How these changes affected surface ocean temperatures in the North Atlantic and ocean water stratification remains poorly constrained. In this study, we apply clumped-isotope thermometry to well-preserved planktonic foraminifera, that are associated with lower mixed-layer to subthermocline dwelling depths from the drift sediments at international ocean discovery program Site 1411, Newfoundland, across four intervals bracketing the EOT. The thermocline/lower mixed-layer dwelling foraminifera record a cooling of 1.9 ± 3.5 K (mean ± 95% CI) across the EOT. While the cooling amplitude is similar to previous sea surface temperature (SST) reconstructions, absolute temperatures (Eocene 20.0 ± 2.9°C, Oligocene 18.0 ± 2.2°C) appear colder than previous organic proxy reconstructions for the northernmost Atlantic extrapolated to this location. We discuss seasonal bias, recording depth, and appropriate consideration of paleolatitudes, all of which complicate the comparison between SST reconstructions and model output. Our subthermocline dwelling foraminifera record a larger cooling across the EOT (Eocene 19.0 ± 3.5°C, Oligocene 13.0 ± 3.2°C, cooling of 5.5 ± 4.6 K) than foraminifera from the thermocline/lower mixed-layer, consistent with global cooling and an increase in ocean stratification which may be related to the onset or intensification of the Atlantic meridional overturning circulation.

Plain Language Summary During the Eocene temperatures on Earth were much warmer than today. It is generally believed that the Antarctic ice-sheet first developed around 34 million years ago, during the Eocene-Oligocene transition (EOT). How this change occurred is still widely debated, but it was probably caused by decreased CO_2 levels and changes to heat distribution through ocean currents. Here, we study how water temperatures at the dwelling depths of planktonic microfossils in the Atlantic Ocean changed across this event. We use clumped isotopes—a way of reconstructing the temperature from fossil shells. We measured shells of planktonic foraminifera, single-celled microscopic plankton, that lived at two different depth levels in the upper ocean. We find that the foraminifera with a shallower (thermocline/lower mixed-layer) water dwelling depth in the North Atlantic Ocean cooled by about ~1.9 K, while those that dwelled deeper cooled by ~5.5 K across the EOT. The thermocline/lower mixed-layer cooling is similar in magnitude to reconstructions from organic biomarkers. However, our reconstructed absolute temperatures are colder than previous estimates. We think that our deeper water temperature reconstructions reflect global cooling, while thermocline/lower mixed-layer temperatures did not cool as much because a warm water current developed, similar to the Gulf Stream.

Key Points:

- Clumped isotopes from well-preserved planktonic foraminifera imply 1.9 K lower mixed-layer/thermocline cooling across Eocene-Oligocene transition (EOT) in North Atlantic
- Our thermocline temperatures for Eocene (20°C) and Oligocene (18°C) are cooler than organic proxy sea surface temperature estimates
- Increased subthermocline cooling compared to the thermocline indicates increased stratification across the EOT, hinting at intensified Atlantic meridional overturning circulation

Supporting Information:

Supporting Information may be found in the online version of this article.

Correspondence to:

I. J. Kocken,
ikocken@hawaii.edu

Citation:

Kocken, I. J., Nooteboom, P. D., van der Veen, K., Coxall, H. K., Müller, I. A., Meckler, A. N., & Ziegler, M. (2024). North Atlantic temperature change across the Eocene-Oligocene transition from clumped isotopes. *Paleoceanography and Paleoclimatology*, *39*, e2023PA004809. https://doi.org/10.1029/2023PA004809

Received 17 NOV 2023
Accepted 29 FEB 2024

Author Contributions:

Conceptualization: Martin Ziegler
Data curation: Helen K. Coxall, Inigo A. Müller, A. Nele Meckler, Martin Ziegler
Formal analysis: Ilja J. Kocken, Kasper van der Veen
Funding acquisition: A. Nele Meckler, Martin Ziegler
Investigation: Ilja J. Kocken
Methodology: Inigo A. Müller, Martin Ziegler
Project administration: Martin Ziegler
Software: Ilja J. Kocken, Peter D. Nooteboom

1. Introduction

Arguably one of the biggest climate changes in the Cenozoic is the Eocene-Oligocene transition (EOT; ~34 Ma, lasting ~500 kyr), which reflects the onset of semi-permanent Antarctic glaciation (see Coxall & Pearson, 2007; Hutchinson et al., 2021; Westerhold et al., 2020, for reviews). The growth of the Antarctic ice-sheet coincides with a shift to higher values in both oxygen isotope ratios ($\delta^{18}O$, ~1‰) and carbon isotope ratios ($\delta^{13}C$, ~0.5‰) of benthic foraminifera (e.g., Westerhold et al., 2020; Zachos et al., 2001, 2008). This onset was associated with a drop in atmospheric CO_2 from ~910 to 560 µl L^{-1} (approximately 1.6× reduction according to Hutchinson

Supervision: Inigo A. Müller, A. Nele Meckler, Martin Ziegler
Validation: Ilja J. Kocken, Helen K. Coxall, Inigo A. Müller, Martin Ziegler
Visualization: Ilja J. Kocken, Peter D. Nooteboom
Writing – original draft: Ilja J. Kocken
Writing – review & editing: Ilja J. Kocken, Peter D. Nooteboom, Helen K. Coxall, Inigo A. Müller, A. Nele Meckler, Martin Ziegler

et al., 2021). The impact of Antarctic ice-sheet growth on Northern Hemisphere temperatures is debated (Goldner et al., 2014; Hutchinson et al., 2021; Liu et al., 2018). In particular, potential contemporaneous changes in the Atlantic meridional overturning circulation (AMOC) may have played an important role in driving water temperature change in the North Atlantic across the EOT (Hutchinson et al., 2019).

In the modern ocean AMOC plays an important role in North Atlantic temperatures due to the associated northward heat transport from lower latitudes in the surface branch of this large scale circulation pattern. An emerging offset in deep sea oxygen isotope composition between the Atlantic and Pacific Ocean after the EOT has been interpreted as a consequence of Northern Component Water formation in the North Atlantic (Cramer et al., 2009). Additionally, changes in the benthic foraminifera assemblage as well as an increased isotopic gradient between surface and deep water in the Labrador Sea have been interpreted as AMOC initialization or intensification up 1 Myr prior to the EOT (Borrelli et al., 2014; Coxall et al., 2018; Kaminski & Ortiz, 2014). An ocean model demonstrated that this onset could be triggered by tectonic Arctic-Atlantic gateway shallowing, which blocked freshwater inflow from the Arctic (Hutchinson et al., 2019). Other models have initiated AMOC onset through CO_2 drawdown and Antarctic Ice Sheet formation (Goldner et al., 2014), shallowing of the Greenland Scotland Ridge (Stärz et al., 2017; Straume et al., 2022), and changes in Southern Ocean Gateways (Elsworth et al., 2017). AMOC intensification is expected to influence meridional heat transport, making it relevant to sea surface temperature (SST) development in the North Atlantic.

Most of the available North Atlantic EOT SST reconstructions to date were generated using the organic geochemical proxies $U^{k'}_{37}$ (Liu et al., 2009, 2018) and TEX_{86} (Liu et al., 2009; Śliwińska et al., 2019), which are derived from alkenones produced by haptophytic algae and glycerol dialkyl glycerol tetraether (GDGT) from a.o. the genus *Nitrososphaerota* (formerly known as *Thaumarchaeota*), respectively. Globally, there are only few EOT records available that are calcium carbonate-based: for $\delta^{18}O$ (from molluscs, fish otoliths, and planktonic foraminifera Coxall et al., 2018; Kobashi et al., 2004; Pearson et al., 2008; Piga, 2020; Wade et al., 2012) and Mg/Ca (Bohaty et al., 2012; Lear et al., 2008; Pearson et al., 2007; Wade et al., 2012), and only two using clumped isotope thermometry (Δ_{47}, Petersen & Schrag, 2015; Taylor et al., 2023). See Hutchinson et al. (2021) for a review of EOT temperature reconstructions. The $\delta^{18}O$ proxy depends on assumptions about the isotopic composition of the sea water. Furthermore, $\delta^{18}O$ values measured on for example, planktonic foraminifera are susceptible to early diagenetic overprinting at the sea floor, resulting in "frosty" foraminifera that are cold-biased (Sexton et al., 2006) whereas reconstructions from Mg/Ca are susceptible to dissolution and carbonate ion effects (Regenberg et al., 2014). However, sites that are clay-rich are able to preserve glassy foraminifera, archiving the original test's formation temperature (Pearson et al., 2001; Sexton & Wilson, 2009; Sexton et al., 2006). One such Site, located on the Newfoundland drift margin, has been shown to preserve Eocene planktonic foraminifera particularly well (Leutert et al., 2019).

Here we reconstruct international ocean discovery program (IODP) Site U1411 temperatures across the EOT based on clumped isotope thermometry. We use well-preserved planktonic foraminifera that are associated with the thermocline/lower mixed-layer and with the subthermocline. Clumped isotope thermometry allows us to generate new temperature constraints for the North Atlantic that are independent from the isotopic composition of the sea water ($\delta^{18}O_{sw}$) for different water depths.

2. Material

2.1. Stratigraphy

Sample material was collected from four target intervals from IODP Site U1411, located at 41°37.1′N, 49°0′W (Norris et al., 2014). We aim to characterize the development of the EOT in broad terms: (a) the late Eocene, (b) the late Eocene just before the earliest Oligocene oxygen isotope step (EOIS), (c) the early Oligocene at the start of the early Oligocene glacial maximum (EOGM), and (d) the Oligocene at the end of the EOGM, or possibly shortly thereafter. The goal is to establish average temperatures well before and after the EOT to determine the temperature change associated with the rapid $\delta^{18}O$ shift that occurs during the EOIS.

We use the age model from the Neptune database (Renaudie et al., 2020), which is an adaptation of the shipboard age model (Norris et al., 2014) that is based on biostratigraphic events as well as two paleomagnetic reversals (Figure S3 in Supporting Information S1).

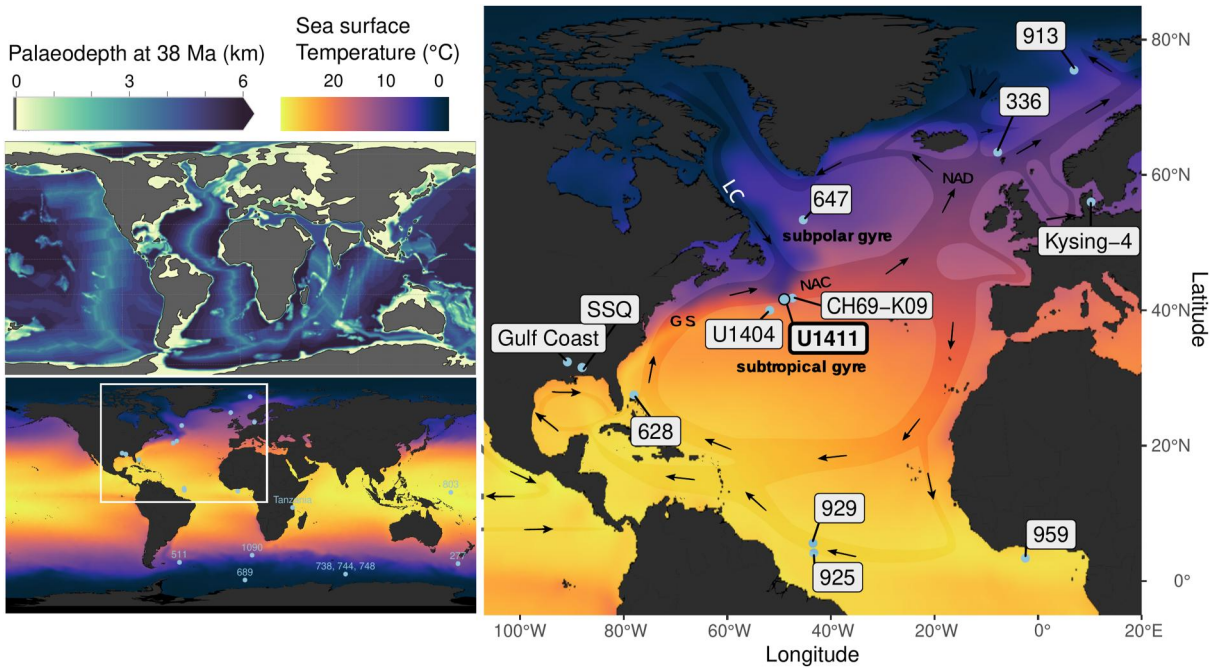

Figure 1. Modern WOA18 annual mean sea surface temperature (Locarnini et al., 2019) with site locations for study sites with Eocene-Oligocene transition data in the Atlantic (right panel, bottom left panel shows world, Hutchinson et al., 2021). The global paleobathymetry of Baatsen et al. (2016) is shown in the top left panel. Study Site U1411 is located on the Newfoundland margin and in the modern ocean is affected by the Labrador Current from the North and the Gulf Stream from the South. This may have been different in the geologic past (see paleobathymetry inset), where the isthmus was open, affecting ocean circulation. Ocean current cartoon adapted from De Schepper et al. (2013). NAC = North Atlantic Current, NAD = North Atlantic Drift.

Modern SSTs (depth of 0 m) at this site fluctuate between ~9.6 ± 25.0°C and 19.9°C seasonally (large uncertainties, few datapoints), with an annual average of 14.4 ± 3.5°C (from the World Ocean Atlas (WOA) Locarnini et al., 2023) and are influenced by surface waters from the Labrador Current (LC) as well as the Gulf Stream (GS) (Figure 1). Note that when we compare our thermocline/lower mixed-layer dwelling foraminifera to modern temperatures, we refer to the estimated dwelling depth of the foraminifera of 25–200 m (average of 80.9 m because of the depth layers in the WOA) instead of SST (see Section 2.2). Here, the annual average temperatures were 11.6 ± 3.0°C. For comparison with the subthermocline, we use the modern ocean temperatures at this site between 200 and 700 m deep (average of 412 m in WOA), which are 7.3 ± 1.2°C (Figure 2).

2.2. Planktonic Foraminifera

Foraminifera species were identified based on the frameworks presented in Pearson et al. (2006), Pearson and Wade (2015), Wade, Olsson, Pearson, Huber, and Berggren (2018), with the Masters' thesis of Holmström (2016) as well as Coxall et al. (2018) for a local perspective on the taxonomy. The most abundant planktonic foraminifera species that were identified in the samples near the EOT are listed in Table 1.

Unfortunately, the surface dwelling foraminifera *T. ampliapertura* and the shallow genera *Pseudohastigerina* and *Globoturborotalita*, which have provided EOT SST signals in previous studies (e.g., Coxall et al., 2018, 2021; Pearson et al., 2008; Wade et al., 2012; see also Figure S4 in Supporting Information S1) were rare in the assemblages, as suggested by the species counts for the late Eocene of Site U1411 (Holmström, 2016).

The clumped isotope method requires large numbers of foraminifera specimens, either within a single sample or between samples for pooling material and achieving the necessary replicate analyses. Thus, generating a monospecific upper mixed-layer SST signal at Site U1411 was not possible. Our approach, therefore, was to generate a "thermocline/lower mixed-layer" signal using a mixture of the most abundant shallower dwelling species. This comprised *T. ampliapertura* where possible, together with the deeper dwelling genera *Dentoglobigerina* and *Subbotina*. We also measured the thermocline to subthermocline dwelling species *C. unicavus* and *C. dissimilis* (Figure 3 and Table S1 in Supporting Information S1).

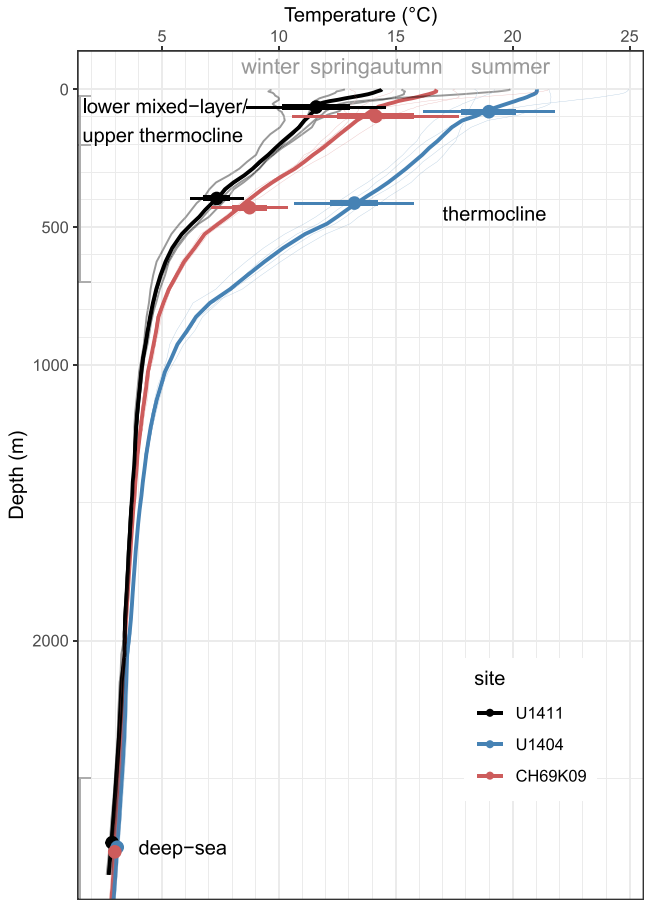

Figure 2. Modern seasonal (thin lines) and annual average (thick lines) temperature profiles of the North Atlantic interpolated to sites U1411 (black), U1404 (blue), and CH69-K09 (red). Indicated depth ranges (gray bars) reflect assumed (sub)thermocline and thermocline/lower mixed-layer foraminifera dwelling depths for comparison to modern ocean temperatures. Point estimates with error bars (68% and 95% CI) indicate the mean of the annual average for the indicated depth interval. All data are from the WOA23 (Locarnini et al., 2023).

Based on extinct foraminiferal carbon and oxygen isotope compositions, the species we study have been previously associated with various dwelling depths (e.g., Pearson & Wade, 2015; Wade & Pearson, 2008; Wade, Olsson, Pearson, Huber, & Berggren, 2018; Wade et al.,2018b). The dwelling depths of these extinct species are not well-constrained, as they rely on the relative distribution of $\delta^{18}O$ and $\delta^{13}C$ values in the assemblages. Isotopic offsets between these species appear to be regionally and/or temporally variable and are associated with some uncertainty, although reproducible patterns are generally found in late Eocene and early Oligocene multi-species stable isotope comparisons (Boersma et al., 1987; Coxall & Spezzaferri, 2018; Moore et al., 2014; Pearson et al., 2001).

We group our results based on previously inferred dwelling depths (Table 1) as well as a separation on the $\delta^{18}O$ signature. Because the *T. ampliapertura* group were relatively rare in the assemblage (Coxall et al., 2018; Holmström, 2016) our *Turborotalia* and *Dentoglobigerina*-dominated assemblage likely reconstruct a lower mixed-layer/upper thermocline signal, whereas the *Catapsydrax* specimens likely reflect a thermocline to subthermocline signal. We label the two groups "thermocline/lower mixed-layer" and "subthermocline." The deeper-dwelling foraminifera still show a distinct $\delta^{18}O$ signature from benthic foraminifera (Coxall et al., 2018). Therefore, we argue that they must have dwelled somewhere near the base of the thermocline (not below it, Figure 2), with the other assemblage of species dwelling shallower in order to account for the large offset in both $\delta^{18}O_{cc}$ and Δ_{47}-based temperatures during the early Oligocene, potentially with a seasonal bias to enhance the contrast. Unfortunately, there was an accidental inclusion of at least a few deeper dwelling foraminifera species in our thermocline/lower mixed-layer assemblage (Figure S1 in Supporting Information S1), which indicates that these temperature estimates may be slightly cold-biased. This effect is likely small however, because of the large number of foraminifera specimens picked for analysis. Despite initial issues with the taxonomy, we are confident that the revision lead to two water masses: samples that represent the subtermocline (dominated by *Catapsydrax*) and the re-evaluated species mixture that comprises thermocline and mixed-layer dwellers. This confidence is warranted by the clear separation of the $\delta^{18}O$ signal after the EOT.

Since clumped isotope analysis requires many replicate measurements to get an accurate statistical average value, samples were measured from three size

Table 1
Foraminifera Species Dwelling Depths Derived From Oxygen and Carbon Isotope Compositions (B. Huber et al., 2016)

Species	Associated dwelling depth	Original reference
S. corpulenta	Thermocline	Wade, Olsson, Pearson, Edgar, et al. (2018)
S. projecta	Thermocline	Wade, Olsson, Pearson, Edgar, et al. (2018)
T. ampliapertura	Mixed-layer	Wade and Pearson (2008)
T. increbescens	Mixed layer	Pearson et al. (2018)
T. cerroazulensis	Shallow subsurface, deeper than *T. ampliapertura*	Pearson et al. (2006)
D. galavisi	Thermocline	Wade, Pearson, et al. (2018)
D. venezuelana	Near-surface (pre-adult) Thermocline (adult)	Wade, Pearson, et al. (2018)
C. unicavus	Thermocline to subthermocline	Coxall and Spezzaferri (2018)
C. dissimilis	Subthermocline	Coxall and Spezzaferri (2018)

Note. See also Figure S4 and Table S1 in Supporting Information S1.

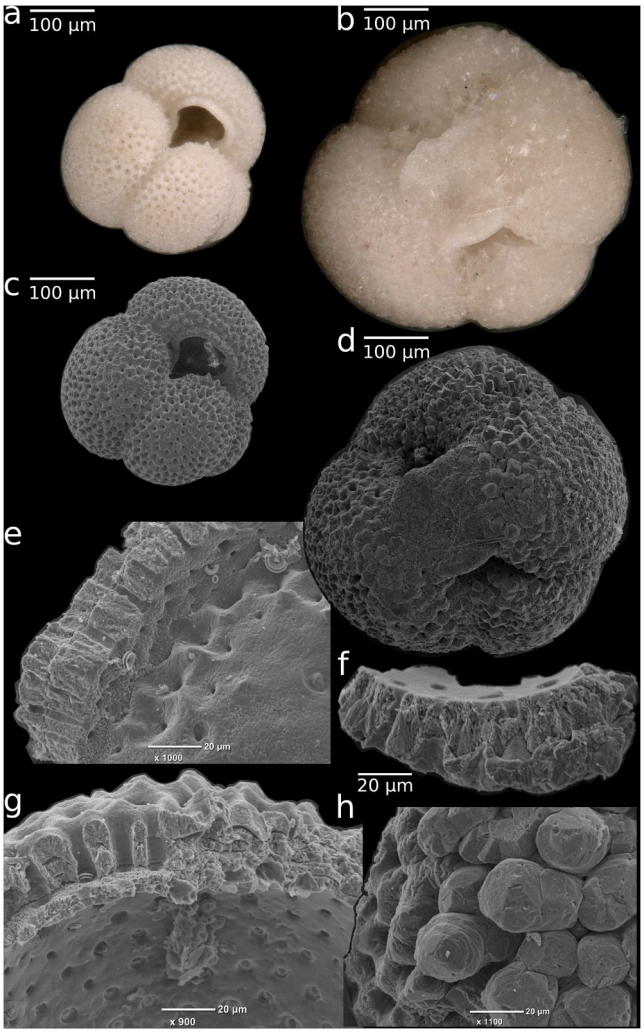

Figure 3. Color (a, b) and SEM photographs (remainder) of *Dentoglobigerina taci/tapuriensis* from sample U1411B 16H5 70–72 cm (IK2-010, left column) and *Catapsydrax* dissimilis from sample U1411C 5H1 60–62 cm (IK1-003, right column). (e–g) Broken sections reveal the original calcite laying in test wall construction, and wall-spanning pores, all exquisitely preserved. (h) Zoomed surface view of *C. dissimilis* showing the nodular morphology or surface thickenings characteristic of this heavily calcified species. Overall we observed little to no dissolution or recrystallization consistent with Leutert et al. (2019).

fractions (150–250, 250–355, and >355 µm). Results derived from the different size fractions were similar and were averaged to provide more replicates and tighter constraints (Figure S10 in Supporting Information S1). Based on the similarity between $\delta^{18}O$ results before and after the EOT (Figure 4 and Figure S4 in Supporting Information S1), subthermocline and thermocline/lower mixed-layer results were averaged separately for the Eocene and for the Oligocene clumped isotope results in order to arrive at more accurate temperature estimates.

Foraminiferal $\delta^{18}O_{cc}$ and Δ_{47} data, especially from planktonic foraminifera, are sensitive to post-depositional dissolution and re-crystallization (Pearson et al., 2001). Many planktonic foraminifera isotope data from previous studies have had to be discarded as recording recrystallized, non-primary signals. Therefore, we took particular care to select a site with excellent preservation of foraminifera (Leutert et al., 2019). The foraminiferal tests showed original micro-structures and pores and rarely displayed secondary crystals (Figure 3).

2.3. Modern Foraminifera Dwelling Depths and Temperatures

Similar to all biologic water column proxy carriers, planktonic foraminifera grow for a limited time and record temperatures of their growing season (e.g., Tolderlund & Bé, 1971). Planktonic foraminifera species have a preferred temperature range that they can tolerate, where the species that occur in the midlatitudes tend to have a larger range of tolerance than those in the tropics (Kucera, 2007). Those foraminifera that dwell in the mixed-layer are known to calcify mostly during the spring bloom (e.g., Ganssen & Kroon, 2000). Dwelling depths of modern planktonic foraminifera can be established from plankton hauls at various depths. Some studies indicate that almost no modern foraminifera live in the top 25 m (Rebotim et al., 2017). When comparing our thermocline/lower mixed-layer dwelling foraminifera results to modern temperatures in the WOA data, we therefore make the comparison to spring 25–200 m deep temperatures (average of 80.9 m because of the depth layers in the WOA) instead of annual average SST. This WOA spring lower mixed-layer temperature at Site U1411 is 11.3 ± 5.8°C. This is fairly similar to the annual average temperature at this depth (the annual average is 11.6 ± 3.0°C) (Locarnini et al., 2023).

The subthermocline temperature does not change seasonally, so foraminifera that calcify at this depth or deeper reflect an annual average temperature. At Site U1411 we define the thermocline depth range as 200–700 m (Figure 2). We filter the WOA data between 200 and 700 m (average of 412 m in WOA) when comparing to our subthermocline dwelling foraminifera, which corresponds to a temperature of 7.3 ± 1.2°C in the modern ocean (Locarnini et al., 2023). Because we measure many replicates consisting of most of the planktonic foraminiferal material in the samples, with enough (≥22) replicates from the different dwelling depths, there is a smaller chance of our results being affected by species-specific caveats.

3. Methods

3.1. Sample Preparation

IODP samples of 7 or 10 cm^3 were freeze-dried, washed with deionized water, wet-sieved into 38–63, 63–150, and >150 µm fractions and dry-sieved into 150–250, 250–355, and >355 µm fractions. Foraminifera specimens were picked from fraction 250–355 and >355 µm by species, typically until sample depletion, using a Nikon SMZ800 with SCHOTT KL 1500 LCD light source with a painting brush wet with deionized water. If there were enough foraminifera of the same species to get a measurement, this typically resulted in something on the order of 10 to 30 specimens per sample.

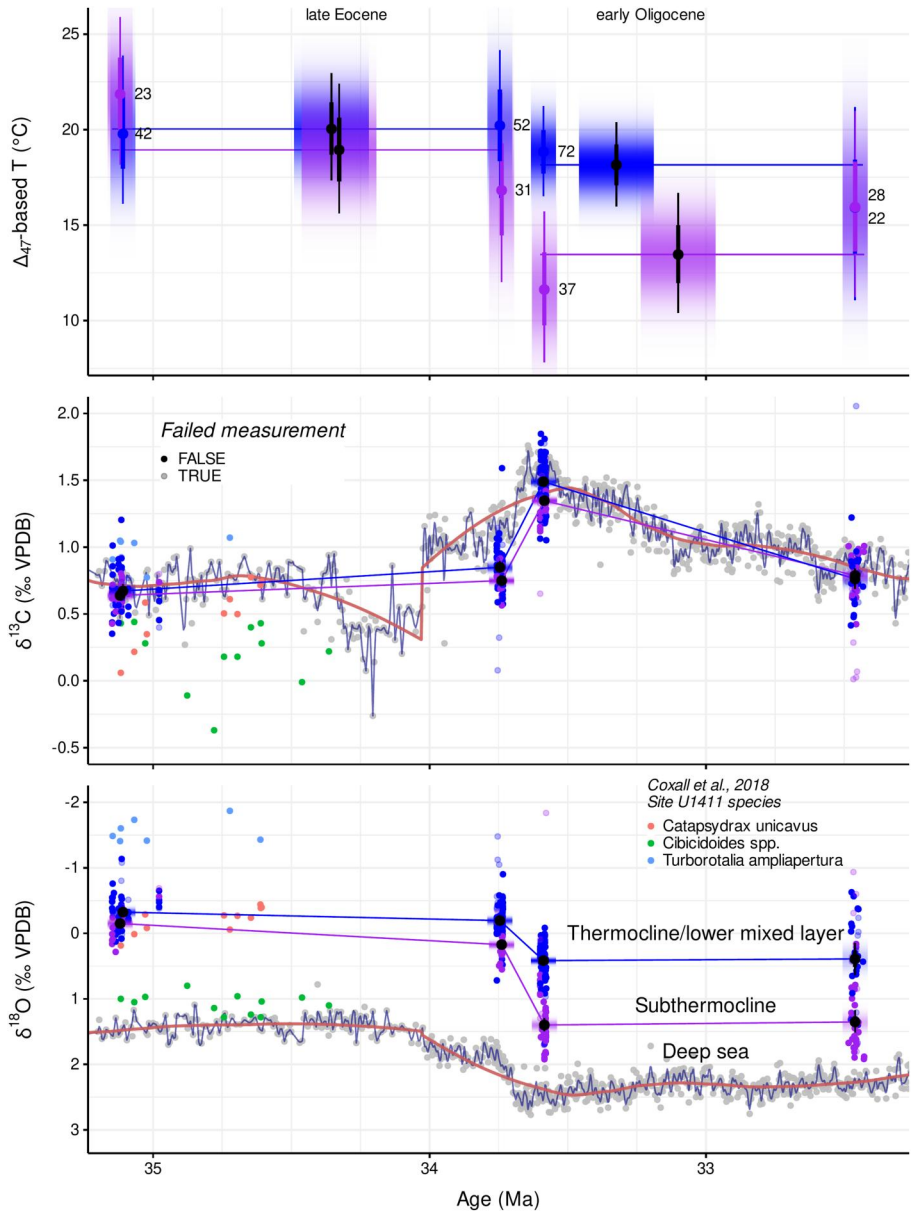

Figure 4. Stable oxygen (δ^{18}O), carbon (δ^{13}C) and clumped (Δ_{47}) isotope composition across the Eocene-Oligocene transition. Clumped isotopes record different amounts of cooling for the thermocline/lower mixed-layer (blue) and the subthermocline (purple). Individual replicates are shown for δ^{13}C and δ^{18}O (points) but not for Δ_{47} because of the large instrumental noise. Replicates that were marked as failed measurements are shown as more transparent points. We show bootstrapped means ±68 and 95 % CIs for each time period and dwelling depth (points with thick and thin error bars) with the number of replicates and the probability density function (gradient) as well as late-Eocene and early Oligocene averages (black points with errorbars and PDF gradients, horizontal lines indicate age ranges). We show Eocene pilot data from the same site for δ^{18}O and δ^{13}C (Coxall et al., 2018). Deep-sea δ^{13}C and $\delta^{18}O_{cc}$ data (gray dots and 1 Myr (red) and 200 kyr (blue) moving averages) are from Westerhold et al. (2020).

Foraminifera were gently crushed between two glass plates and cleaned with deionized water in an ultrasonic bath for 20 s. Some samples were prepared at Utrecht University (UU) and some at Bergen University (UiB). Those that were prepared at UiB were also rinsed with 200 µl of MeOH prior to ultrasonication. This rinse was skipped for all subsequent measurements at UU since valuable sample material is often lost during the rinsing and there were no visible differences between samples cleaned with or without MeOH. Replicates were weighed between 70 and 95 µg for measurement.

3.2. Microscopy

Color photographs were made using a Keyence VHX-5000 digital microscope. In order to investigate planktonic foraminifera preservation and the efficacy of the cleaning procedure, both cleaned and uncleaned samples were prepared for SEM imaging by placing foraminiferal tests or fragments on a stub with a two-sided carbon sticker and adhering 4 nm of Pt/Pd-target. Images were generated on a JEOL-Neoscope JCM6000 Benchtop SEM. The figure panels in Figure 3 were created by manually cutting out the foraminifera from the background and laying them out in Inkscape (Inkscape Project, 2021).

3.3. Clumped Isotope Analysis

3.3.1. Measurement

The sample and standard aliquots were measured on a Kiel IV carbonate device modified with a custom-built Porapak trap with a Thermo Fisher MAT 253 plus isotope-ratio mass spectrometer in the laboratories of UU and UiB. The method we used was first introduced in Schmid and Bernasconi (2010) and is described in detail in Meckler et al. (2014). In short, samples were dissolved at 70°C in hypersaturated phosphoric acid (H_3PO_4) in a vacuum. The released gas was purified in two consecutive cold traps interspersed with a manually installed 4 cm Porapak Q bracketed by 1 cm of silverwool kept at −15°C (UiB, using Peltier elements) and −40°C (UU, using a custom-built liquid nitrogen cooling system).

We measured the aliquots in microvolume mode with 40 10 s cycles using the long-integration dual inlet approach (Hu et al., 2014; I. A. Müller, Fernandez, et al., 2017).

3.3.2. Carbonate Standards

In a single run of measurements, we measured 46 aliquots comprising 20 samples and 26 standards. We used the carbonate standards ETH-1, ETH-2, ETH-3 to convert the measurements to the absolute reference frame (Dennis et al., 2011) with long "sessions" for which we assume that the apparatus is stable. We used the accepted standard values on the I-CDES scale from Bernasconi et al. (2021), who describe carbonate-standardization in detail.

Standards at UiB were measured in equal proportions between ETH-1, ETH-2, ETH-3, and ETH-4 at the time of measurements. At UU, we measured many more ETH-3 standards, since they are much closer to the likely sample Δ_{47} values (Kocken et al., 2019) and allow for intra-run drift correction, dubbed "offset correction" here.

Check standards ETH-4, IAEA-C2, and Merck were measured to establish long-term reproducibility and to monitor the application of the pressure-baseline correction (Bernasconi et al., 2013; He et al., 2012; Meckler et al., 2014).

3.3.3. Data Processing

Raw Isodat measurement and scan data were read into memory using the programming language R (R Core Team, 2020) using the package `isoreader` (Kopf et al., 2021) and processed using `clumpedr` (Kocken, 2019). The UU-specific code is archived at (Kocken, 2022). We read in the raw measurement files as well as the daily background scans, implemented metadata fixes, additions, and files manually marked as outliers based on machine errors. We calculated the pressure-baseline correction models, which relate local minima in the masses 45 through 49 to the maxima in mass 44 via a third order polynomial (Bernasconi et al., 2013; He et al., 2012; Meckler et al., 2014). These models were then used to correct the raw intensity data of the measurements scaled by a factor of 0.9–1 (for different time periods) for UU and 1 for UiB to minimize the difference between raw ETH-1 and ETH-2 Δ_{47} values (Meckler et al., 2014; I. A. Müller, Violay, et al., 2017). This is done because we know that the clumped isotope composition of ETH-1 and ETH-2 should be very similar as they were heated at identical elevated temperature conditions to near-stochastic isotope composition, and differences between the two are thus likely the result of uncorrected background effects (Bernasconi et al., 2018).

Measurements with sudden drops in the intensity of the signal (which typically occurs when the previous measurement fails on our Kiel IV device) were automatically (partially, from the drop onward) marked for exclusion when the pressure drop was more than three times the first cycle drop in pressure. Then, the cycles were summarized for each sample. Samples were marked as failed measurements based on initial mass 44 intensity (below 8 V, greater than 30 V, difference between reference gas and sample gas greater than 3 V).

A rolling offset correction (`expected value − raw value`) was applied within each run to correct for intra-run drift, with a window size of 7 using ETH-3 only for Δ_{47} and a window size of 15 for $\delta^{18}O$ and $\delta^{13}C$ using ETH-1, ETH-2, and ETH-3.

To correct for scale-compression an empirical transfer function (ETF) was calculated (Dennis et al., 2011), which fits a line to the raw values as a function of accepted standard values (Bernasconi et al., 2021), and applies this conversion in reverse to all raw Δ_{47} data. We used standards ETH-1, ETH-2, and ETH-3 for the ETF, defining three distinct long sessions (Figure S9 in Supporting Information S1). The two sessions at UU were defined as 23 February 2018 to 21 December 2019 and from 3 January 2020 to 22 January 2021 and consist of respectively 7,859 and 3,584 measurements. At UiB, the session ranged from 21 August 2018 to 9 September 2018 and consisted of 405 measurements.

As mentioned earlier, replicate analyses for the two dwelling depths and the four time intervals, as well as pre-EOT and post-EOT were statistically averaged so that a sufficient number of replicates was attained to quantify the uncertainty of the mean value robustly. We do this using bootstrapping, so that the uncertainty distribution of the mean can be easily propagated and incorporate the uncertainty from the temperature equation (Kocken, 2023).

3.3.4. Reproducibility of Stable Isotope Measurements

At UU, the $\delta^{13}C$ reproducibility of the independent check standard IAEA C2 was 29.6 and 36.9 ppm (standard deviation, $N = 251$ and 113) for the two sessions. For $\delta^{18}O$ it was 74.4 and 117.6 ppm and the long-term reproducibility of Δ_{47} was 29.2 and 36.9 ppm.

At UiB, ETH-4 ($N = 33$) was used as a check standard with standard deviations of 13.1 ppm for $\delta^{13}C$, 40.5 ppm for $\delta^{18}O$ and 37.9 ppm for Δ_{47}.

3.3.5. Temperature Calibration

We use the foraminifera calibration from Meinicke et al. (2020), which was recalculated to the I-CDES scale in Meinicke et al. (2021). This calibration includes reprocessed foraminifera data from Peral et al. (2018), which are also available in Peral et al. (2022). While it covers a smaller range of formation temperatures than other calibrations, the linear assumption of the regression is more plausible for the smaller interval. An alternative could be the Anderson et al. (2021) calibration, which includes biogenic, abiogenic, and synthetic carbonates and covers a much larger temperature range. However, it appears that at the high temperature range in the Anderson et al. (2021) calibration, the clumped isotope values may be higher than expected from a linear fit. Using the Meinicke et al. (2021) calibration in favor of the Anderson et al. (2021) calibration results in final temperature reconstructions that are 1.520 ± 0.004°C warmer (based on the difference for formation temperatures of −5 to 30°C, clumped isotope values between 0.587 and 0.704‰ I-CDES, Figure S6 in Supporting Information S1). Both calibrations are based on the newest accepted values for the carbonate standards from Bernasconi et al. (2021) that were determined via heated and equilibrated gases in several laboratories.

Uncertainty from the temperature regression is included in the final temperature estimates via a bootstrapped Monte-Carlo estimation from slope-intercept pairs from Meinicke et al. (2021) re-implemented in R (Kocken, 2023), even though it has a minor influence in the final uncertainty estimates.

3.4. Calculating $\delta^{18}O_{sw}$

The independent temperature estimates from Δ_{47} can be combined with the $\delta^{18}O_{cc}$ values to calculate $\delta^{18}O_{sw}$ values. We do this by solving the quadratic approximation by Kim and O'Neil (1997) as modified by Bemis et al. (1998) for $\delta^{18}O_{sw}$. This is the recommended calibration according to DeepMIP (Hollis et al., 2019). Note that we also calculate the $\delta^{18}O_{sw}$ by using the equations from Erez and Luz (1983), Marchitto et al. (2014), Shackleton (1974) in Figure S5 in Supporting Information S1.

As such, the isotopic ratio of the seawater ($\delta^{18}O_{sw}$) is calculated by:

$$\delta^{18}O_{sw} = \frac{\sqrt{-4 \times 16.1 \times 0.09 + (-4.64)^2 + 4 \times 0.09T} - 4.64 + 2 \times 0.09\delta^{18}O_{cc}}{2 \times 0.09} + 0.27 \quad (1)$$

where T is the temperature in °C, $\delta^{18}O_{cc}$ is in Vienna Pee Dee Belemnite (VPDB) (hence the 0.27) and $\delta^{18}O_{sw}$ is in Vienna Standard Mean Ocean Water (VSMOW).

Uncertainty in the parameters in this equation is ignored in our final $\delta^{18}O_{sw}$ error estimates, as it is poorly constrained and is likely dwarfed by uncertainties in Δ_{47} values.

3.5. Modeling Foraminifera Advection

Recent ocean model simulations of the middle Eocene (38 Ma) with a higher resolution than usual (0.1° compared to 1° or coarser, Nooteboom et al., 2022) allow us to use virtual, sinking Lagrangian particles to assess the lateral transport of planktonic foraminifera (van Sebille et al., 2015). The small scales that are resolved in these simulations are important to obtain a realistic time-mean flow (Marzocchi et al., 2015; Porta Mana & Zanna, 2014) and eddies, resulting in a representative transport of these virtual particles (Nooteboom et al., 2020). Virtual particles were released every five days for a period of 2 years at the bottom of the ocean in eddying ocean model (0.1° horizontal resolution) of the late Eocene (38 Ma; $2 \times pCO_2$ forcing) with the paleobathymetry of Baatsen et al. (2016) (Figure 1 top left). Each sinking particle was tracked back in time while advected by ocean currents from the ocean bottom until it reached its dwelling depth. Then the particles were tracked back in time at this dwelling depth during their lifespan. This results in a distribution of near-surface foraminifera origin locations, and the temperatures/salinities they experienced during their journey.

We used two distinct dwelling depths for the particles: a very shallow 50 m (Rebotim et al., 2017) and a deeper 300 m (Groeneveld & Chiessi, 2011). Note that these depths differ from the estimated dwelling depth of our assemblages, which were reassessed during review. For all particles, the sinking speed was estimated at 200 m/d and they were assigned a life-span of 30 d (Takahashi & Be, 1984). Note that the high sinking speed relative to other sinking particles can be adjusted up or down by up to 100 m/d without affecting the results to a large extent, as advective transport during their life time mostly determines the outcome (Nooteboom et al., 2019; van Sebille et al., 2015).

The site's present-day location was translated to the paleobathymetry with the plate reconstructions of van Hinsbergen et al. (2015) using the rotational reference frame of Torsvik et al. (2012) in GPlates (R. D. Müller et al., 2018), to determine the site location at 38 Ma. To cope with uncertainties in this paleo-location, a grid of 14° × 14° in both paleolatitude and paleolongitude was generated around the target site to release particles at the ocean bottom. This allows us to test the spatial sensitivity of the backtracking analysis on the paleolatitude/paleolongitude. A total of 28,616 particles were used in one particle back-tracking simulation (i.e., for each dwelling depth used).

4. Results

As expected, the planktonic $\delta^{18}O$ data were ^{18}O-depleted in comparison to benthic records (Westerhold et al., 2020, note that they are not from the same site, however) but showed a similar amplitude of change across the EOT (Figure 4). Prior to the EOT, the subthermocline dwelling foraminifera showed a similar $\delta^{18}O$ (−0.15 ± 0.08‰) value to the thermocline/lower mixed-layer dwelling foraminifera (−0.32 ± 0.08‰, Figure 4). The $\delta^{18}O$ of the subthermocline dwelling foraminifera increased to 0.17 ± 0.07‰ approaching the EOT while the thermocline/lower mixed-layer foraminifera changed to −0.19 ± 0.07‰. Shortly after the EOT the offset in $\delta^{18}O$ between subthermocline dwellers (1.40 ± 0.10‰) and thermocline/lower mixed-layer species (0.42 ± 0.06‰) increased. In the early Oligocene, the $\delta^{18}O$ of the subthermocline dwelling foraminifera remained offset (1.40 ± 0.16‰), while the thermocline/lower mixed-layer foraminifera recorded 0.39 ± 0.25‰.

The $\delta^{13}C$ values are similar between the subthermocline dwellers and the thermocline/lower mixed-layer dwellers throughout the record, with the largest offsets (of ∼0.14‰) just before and after the EOT (Figure 4). On average, the thermocline to mixed-layer $\delta^{13}C$ values change from 0.66 ± 0.04‰ to 0.81 ± 0.04‰, then increase to 1.40 ± 0.04‰ across the transition and then decrease again to 0.78 ± 0.07‰. See Figure S4 in Supporting Information S1 for a crossplot of $\delta^{13}C$ and $\delta^{18}O$ grouped by species assemblage and time-period.

Absolute $\delta^{13}C$ values and changes across the EOT are in agreement with the benthic $\delta^{13}C$ data in Westerhold et al. (2020), with the caveat that the composite record for this interval is based on an astronomical tuning,

Table 2
Clumped Isotope Results Averaged Before and After the Eocene-Oligocene Transition (Bootstrapped Mean ± 95 % Confidence Level)

	Age (Ma)	N	$\delta^{13}C$ (‰ VPDB)	$\delta^{18}O$ (‰ VPDB)	Δ_{47} (‰ I-CDES)	T (°C)	$\delta^{18}O_{sw}$ (‰ VSMOW)
M	34.4	94	0.77 ± 0.04	−0.25 ± 0.05	0.614 ± 0.008	20.0 ± 2.9	0.85 ± 0.60
M	33.3	94	1.32 ± 0.07	0.41 ± 0.07	0.620 ± 0.007	18.2 ± 2.2	1.12 ± 0.47
T	34.3	54	0.70 ± 0.03	0.04 ± 0.07	0.618 ± 0.011	18.9 ± 3.5	0.91 ± 0.70
T	33.1	65	1.11 ± 0.07	1.38 ± 0.09	0.636 ± 0.010	13.5 ± 3.2	1.07 ± 0.70

Note. The average age differs between dwelling depths based on the number and spacing of replicates along the core. *M* = thermocline/lower mixed-layer, *T* = subthermocline.

whereas our age model is based on biostratigraphic events on the GTS 2020 (Speijer et al., 2020). This means that, for example, the subtly lower $\delta^{13}C$ values at ∼33.75 Ma could be the result of age model discrepancies.

We briefly discuss the $\delta^{13}C$ results here, because extensive discussion is beyond the scope of this paper. The general agreement between our planktonic $\delta^{13}C$ data with the benthic record indicates that the carbon cycle perturbation across the EOT represents a global, depth-integrated signal, whereas the $\delta^{18}O$ data show a stratified response across the EOT. A uniform shift in $\delta^{13}C$ has previously been associated with either a shelf-to-basin carbonate shift with highly ^{13}C-enriched shelf carbonates, or a sequestration of ∼1,000 Pg of organic carbon via permafrost and peatland expansion during the EOT (Armstrong McKay et al., 2016).

Clumped isotope-derived temperature estimates are 20.0 ± 4.1, 20.0 ± 4.0, 19.0 ± 2.4, and 16.3 ± 5.3°C (N = 42, 52, 72, and 22, from late Eocene to early Oligocene) for the thermocline/lower mixed-layer dwelling foraminifera and 22.0 ± 4.0, 17.0 ± 5.0, 12.0 ± 4.1, and 16.0 ± 5.0°C (N = 23, 31, 37 and 28) for the subthermocline dwellers (Table S1 in Supporting Information S1). When we average the Eocene and the Oligocene temperatures in order to gain more precise estimates, we obtain Eocene temperatures of 20.0 ± 2.9°C for the thermocline/lower mixed-layer (N = 94) and 19.0 ± 3.5°C for the subthermocline dwelling species (N = 54), while Oligocene temperatures were 18.0 ± 2.2 and 13.0 ± 3.2°C (N = 94 and N = 65) respectively, indicating a cooling of 1.9 ± 3.5 and 5.5 ± 4.6 K for the two dwelling depths (Table 2). Bayesian *t*-tests indicate moderate evidence (Bayes Factor (BF) = 1/3.67) against cooling in the thermocline/lower mixed-layer and anecdotal evidence (BF = 2.24) for cooling in the subthermocline. During the Eocene, there is moderate evidence (BF = 4.89) that the thermocline/lower mixed-layer and the subthermocline had indistinguishable temperatures, while there was moderate evidence (BF = 3.27) for a difference between the dwelling depths during the Oligocene.

The $\delta^{18}O_{sw}$ values for the late-Eocene, pre-EOT, post-EOT, and early-Oligocene are 0.73 ± 0.87‰, 0.95 ± 0.81‰, 1.30 ± 0.50‰, and 0.63 ± 1.10‰ for the thermocline/lower mixed-layer dwelling foraminifera and 1.30 ± 0.79‰, 0.60 ± 1.00‰, 0.60 ± 1.00‰, and 1.6 ± 1.1‰ for the subthermocline dwelling foraminifera (Figure S5 in Supporting Information S1). On average, this results in 0.85 ± 0.60‰ and 1.10 ± 0.47‰ for the thermocline/lower mixed-layer during the Eocene and Oligocene respectively (difference of 0.05 ± 0.89‰). For the subthermocline, we get 0.91 ± 0.70‰ and 1.10 ± 0.70‰ across the transition (difference of 0.05 ± 0.82‰). The uncertainties for these values are large because they inherit the uncertainty from the clumped isotope-derived temperatures, rendering it difficult to distinguish instrumental noise from a primary signal (Table S1 in Supporting Information S1). However, the overall values may indicate an ^{18}O enriched sea water composition compared to expected values, after taking into account ice-volume effects. In the modern ocean $\delta^{18}O_{sw}$ estimates near Site U1411 are around 0 VSMOW near the surface, increase to 0.26 ± 0.09‰ in the mixed-layer and to 0.50 ± 0.08‰ in the thermocline, and ultimately decrease to 0.260 ± 0.03‰ beneath 2 km (Schmidt et al., 1999).

We show in Figure S5 in Supporting Information S1 how the different equations affect the $\delta^{18}O_{sw}$ estimates. They increase the average by up to 0.34 ‰ or decrease it by ∼0.20‰, depending on the equation used. All the averages fall approximately within our 68 % confidence level as determined from the temperature uncertainties when using our preferred equation.

10.1029/2023PA004809

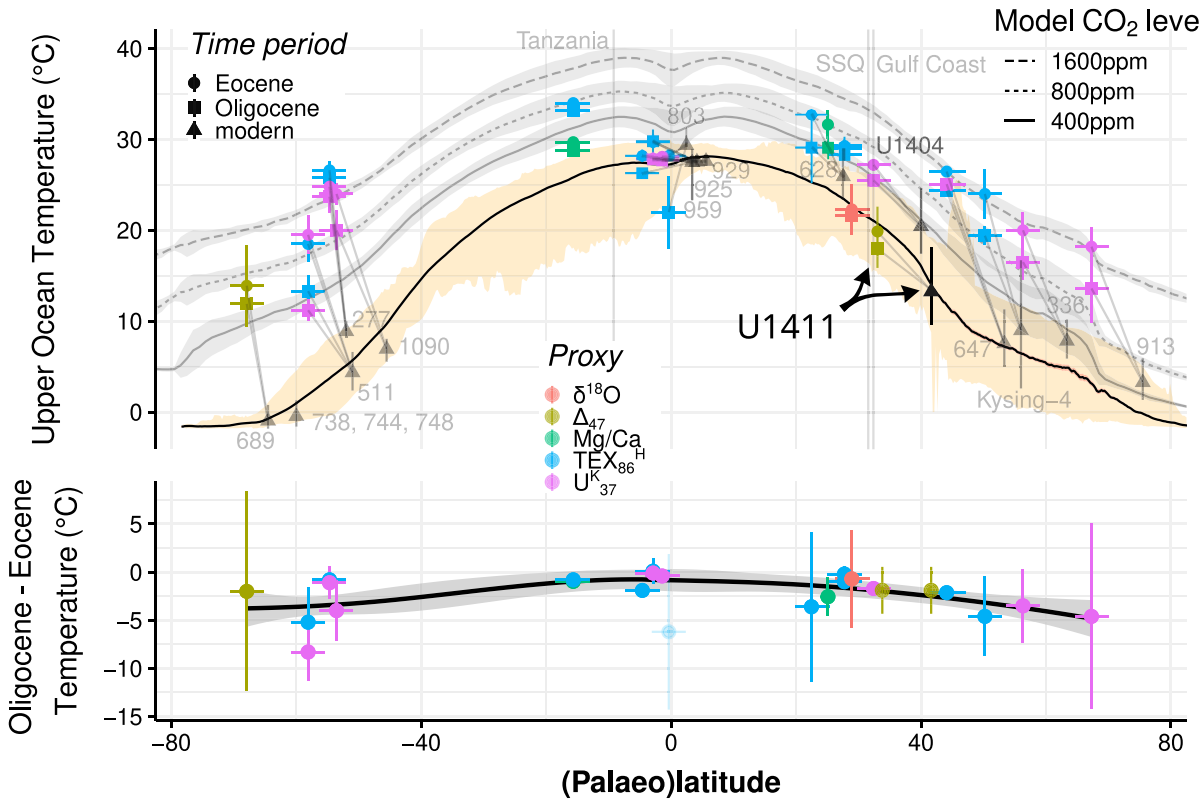

Figure 5. Upper ocean temperature estimates as a function of (paleo)latitude (top panel) for the various proxy records available (colors) (see text, Hutchinson et al., 2021). The modern sea surface temperature variability is indicated as the annual average (line, red shading is the 95% CI, very narrow) and the full range (yellow shaded interval), as well as for the different sites (black triangles and range, vertical gray lines for modern site locations that have no modern ocean temperature in the World Ocean Atlas) (Locarnini et al., 2019). Eocene (circles) and Oligocene (squares) temperature estimates show warmer temperatures at higher latitudes due to polar amplification. Note that a simple comparison of Site U1411 Eocene-Oligocene transition (EOT) reconstructions to the modern SSTs at the site's paleolatitude does not reflect the nuanced context of these changes, because the North Atlantic basin was more restricted (Figure 1) with implications for the oceanography. The 3 model outputs with different levels of CO_2 forcing (1,600 ppm = dashed, 800 ppm = dotted, and 400 ppm = continuous line, all with gray shading) by Hutchinson et al. (2018) illustrate how models cannot reconcile very high polar temperatures with relatively cool tropical temperatures. The proxy cooling across the EOT (bottom panel) is larger at higher latitudes. Horizontal error bars represent the 95% confidence interval of the paleolatitude reconstruction for 34 Ma. Vertical error bars in the top panel represent uncertainties as presented in Hutchinson et al. (2021). In the bottom panel, we recalculated the uncertainties as the mean squared error of the difference. The error bars for our new Site U1411 datapoint represents the 95% confidence interval and the 95% confidence interval of the difference.

5. Discussion

With our clumped isotope analyses on thermocline/lower mixed-layer and subthermocline dwelling foraminifera, we provide absolute temperature estimates spanning the EOT that are independent of the sea water isotope composition. This leads to new insights on the extent of cooling and changes in the upper water column stratification in the North Atlantic.

In the following we discuss these temperature reconstructions in the context of modern conditions at the site location, a proximal site during the Late Holocene and the last glacial maximum (LGM), and to previous SST reconstructions for the EOT. Then we discuss how lateral advection may have influenced the site, and how the oceanography may have evolved across the EOT in terms of ocean stratification and AMOC.

5.1. Comparison to the Modern SST in the North Atlantic

When comparing climate reconstructions to modern ocean temperatures and, importantly, to paleo-climate simulations, the comparison is typically made to a site's paleolatitude, which changes over geologic timescales due to plate tectonics. In the case of Site U1411, the difference between the modern SST for this latitude (~41°N) and its reconstructed paleolatitude for the Eocene (~33°N) bands is ~6.2°C (Locarnini et al., 2019). Site U1411 is a prime example that demonstrates that a simple comparison of reconstructed conditions at the paleolatitude with

a corresponding modern latitudinal average can lead to large biases, where very different oceanographic settings are compared.

In order to compare the reconstructed EOT temperatures with the present day, we argue that the temperatures at the modern site location are a more reasonable reference instead of using the temperatures of a latitude that corresponds to the paleo location. First, the oceanography near Site U1411 is strongly influenced by the bathymetry—in particular the Grand Banks shelf that steers the western intensification of the subtropical and subpolar gyres in the region (Figure 1). Even though the paleolatitude of Site U1411 was further to the South, the position with respect to the main bathymetric features was similar and hence the large-scale features of the oceanography, with influence from the North and South, was likely similar to the modern ocean. Model studies also indicate that the proto GS was located relative to the bathymmetry, not to a particular latitude (e.g., the barotropic stream function shows a similar shape with respect to the bathymmetry in Figure S4 of Nooteboom et al., 2022) The paleolatitude is situated in a very different oceanographic setting in the modern ocean, with a dominant influence of subtropical gyre currents coming from lower latitudes. Furthermore, western boundary circulation is generally warmer than the latitudinal band (Judd et al., 2020), so making the comparison to the present-day latitude of the site rather than the modern ocean temperature at the site location would likely make our reconstructions appear too cold for the latitude.

The EOT sediments of Site U1411 are characterized as muddy drift deposits, derived from fine particles transported from the north, so the sedimentary archive could be biased to northward surface conditions (Boyle et al., 2017). Furthermore, advection in the water column may have affected the temperature signal captured by the foraminifera, at least seasonally, via the GS and the LC. This is also confirmed by model simulations (Nooteboom et al., 2022) (see Section 5.4).

Our temperature reconstructions from Eocene and Oligocene thermocline/lower mixed-layer dwelling foraminifera are respectively ∼8.4 and ∼6.6 K warmer than the modern ocean mixed-layer (depth of 25–200 m) spring temperature near Site U1411 (Figure S15 in Supporting Information S1). The Eocene and Oligocene subthermocline dwelling foraminifera at Site U1411 reconstruct respectively ∼11.6 and 6.1 K warmer temperatures than the modern ocean thermocline annual average temperature (depth of 200–700 m, Figure 2). In view of the warm (up to 20°C) biomarker-based SST reconstructions in the North Atlantic across the EOT (Liu et al., 2009, 2018; Śliwińska et al., 2019) these temperatures appear to be relatively cool (Figure 5). However, we will show in the next sections that the temperatures we reconstruct are reasonable after considering LGM and the Late Holocene reconstructions in the context of reconstructed atmospheric CO_2 concentrations, and climate modeling studies.

5.2. Comparison to the Late Holocene and Last Glacial Maximum (LGM)

Since the comparison between proxy reconstructions and water column temperatures is complex due to uncertainties in seasonality and depth habitat of the proxy carrier, we also compare our data to subrecent coretop and Holocene planktonic foraminifera temperature reconstructions. Furthermore, the lower thermocline/lower mixed-layer planktonic foraminifera assemblage that was needed for this study to measure enough material for clumped isotopes makes this harder still. We assume that they show similar dwelling depths, habitat preferences, and may show similar seasonality preferences. These Holocene reconstructions are based on Mg/Ca and $\delta^{18}O$ and are considered reliable because they are based on well-preserved foraminiferal tests and well-constrained ocean composition for these time periods.

Core-top data from site CH69-K09 (located ∼138 km east of Site U1411 with a slightly warmer (∼2 K) temperature profile, Figure 2) from *G. bulloides* Mg/Ca indicate temperatures of 12.3°C (Riveiros et al., 2016), while *G. inflata* $\delta^{18}O$ data from the same site imply 12.8 and 12.3°C (for two size-fractions, Cléroux et al., 2008). These temperatures are also consistent with an interpretation that the foraminifera capture an average spring temperature of around 81 m deep (which is 13.3 ± 2.3°C between 25 and 200 m at Site CH69-K09 in the modern ocean, Locarnini et al., 2023). Thus, in comparison to site CH69-K09, our late Eocene and early Oligocene thermocline/lower mixed-layer dwelling planktonic foraminifera temperature reconstructions are respectively ∼8.5 and 6.2 K warmer.

To put the temperature change at Site 1411 across the EOT into perspective, we further make a comparison with the temperature change that occurred at this location across the last deglaciation starting at the LGM 20,000 years

ago. Tierney, Zhu, et al. (2020) reconstructed LGM (23 to 19 ka) temperatures of 7.8 ± 0.5°C, based on a proxy ensemble ($\delta^{18}O$, Mg/Ca, $U^{k'}_{37}$, and TEX_{86}) combined with an isotope-enabled climate model. They record a difference of 5.6 ± 1.4 K between the Late Holocene and the LGM. The cooling we observe across the EOT in the subthermocline (5.4 ± 4.6 K) is similar in magnitude, although reversed sign, to the warming that occurred between the LGM and Late Holocene SST. Without discussing potential implications on climate sensitivity in great detail, we note that when comparing these changes simply with associated changes in atmospheric CO_2, our results show a consistent pattern at this location: we record similar cooling between a warmhouse, ice-free world, and a coolhouse with a permanently glaciated Antarctica (using the terminology from Westerhold et al., 2020) with a 1.58-fold CO_2 decrease (from ~885 to 560 ppm, Hutchinson et al., 2021) compared to a 1.56-fold increase (~180–280 ppm) and associated warming from LGM to Late Holocene (Tierney, Zhu, et al., 2020).

5.3. Absolute Clumped-Isotope Based EOT Temperatures Were Cooler Than Previous North Atlantic Reconstructions

Eocene organic proxy records reconstruct warm SST from Atlantic mid-to-low paleolatitudes (10°–40°N, ~27.0 ± 3.2°C, mean 95% CI assuming independent errors) (data compilation from Hutchinson et al., 2021). The organic proxies also reconstruct warm high latitudes for the North Atlantic. For Kysing-4, located at 50.3°N, TEX_{86} data indicate 24.0 ± 2.7°C (Śliwińska et al., 2019). Site 336 and 913, located at 56.4° and 67.5°N, $U^{k'}_{37}$ data reconstruct 20 ± 2 and 18.2 ± 2.2°C (Liu et al., 2009). See Figure 5 and Hutchinson et al. (2021) for a review.

In comparison to the North Atlantic organic proxy reconstructions, our thermocline/lower mixed-layer clumped isotope temperatures from Site U1411 are cooler by about 0.7 K during the Eocene and by ~1.6 K during the Oligocene, although our sampling site is located much farther to the South (Figure 5). Śliwińska et al. (2023) recently reconstructed southern Labrador Sea (ODP Site 647, latitude of 53°20′N) EOT temperatures of 26.4 ± 0.5 to 24.3 ± 0.3°C (Eocene and Oligocene values calculated from their raw data). Their temperature estimates were ~6.4 and 6.2 K warmer than our thermocline/lower mixed-layer reconstructions for the Eocene and Oligocene respectively (~7.5 and 10.8 K warmer than our subthermocline reconstructions), whereas this site's SST is ~4.1 K *colder* than Site U1411 in the modern ocean.

IODP Site U1404 is the closest site for which EOT temperature reconstructions are available. It is located ~297 km South West of U1411 and was analyzed by Liu et al. (2018) using $U^{k'}_{37}$. Their temperature reconstructions for the latest Eocene are warmer by ~7.2 K compared to our estimates for the subthermocline and thermocline/lower mixed-layer. At the beginning of the Oligocene, Site U1411's lower thermocline/lower mixed-layer foraminifera are ~7.4 K cooler than organic geochemical temperature reconstructions for site U1404. In the modern ocean, the temperature difference between sites U1404 and U1411 is ~7.4 K at 25–200 m deep and 5.9 K at 200–700 m (Figure 2, Locarnini et al., 2023), which is similar in magnitude to our observed differences. Therefore, our findings could be compatible with those of site U1404 if we assume that the oceanography was comparable to the modern during the EOT—the subpolar- and subtropical gyre circulated in the same direction—and that the $U^{k'}_{37}$ proxy represents a surface or mixed-layer signal (Liu et al., 2018). However, if we extend the comparison to proxy records farther to the north of our study site and consider the reconstructions for the southern Labrador Sea (ODP Site 647 Śliwińska et al., 2023), it appears that the TEX_{86} proxy captures systematically warmer temperatures than our clumped isotope results (Figure 5). If we go farther north still, $U^{k'}_{37}$ also captures warmer temperatures than we would expect at such a high latitude, given our Δ_{47}-based temperature estimates (Liu et al., 2009). One explanation could be that the TEX_{86} and $U^{k'}_{37}$ capture a signal closer to the surface than our thermocline/lower mixed-layer dwelling foraminifera, or are biased toward the summer season. Otherwise, this discrepancy may have implications for the proxy-model mismatch, where Eocene models are unable to reproduce the low meridional temperature gradient that is inferred from organic proxy records (M. Huber & Caballero, 2011; Hutchinson et al., 2018).

While the offset in absolute temperatures is very large between our reconstructions and those from higher latitudes made with different proxies, the *change* across the EOT is similar, specifically in comparison to the thermocline/lower mixed-layer dwelling foraminifera (Figure 5). The North Atlantic sites Kysing-4, Site 336, and Site 913 record a cooling of ~4.6 ± 2.7, 3.6 ± 2.0, and 4.6 ± 3.8 K respectively (Liu et al., 2009; Śliwińska et al., 2019). At Site U1404, a cooling of ~2 K was recorded (Liu et al., 2018), while Site 647 showed a cooling of ~2.1 ± 0.5 K (calculated from raw data of Śliwińska et al., 2023) across the EOT. At St. Stephens Quarry (SSQ)

(paleolatitude of 27.2°N) (Wade et al., 2012) report a cooling of 2.6 ± 1.6 K from TEX_{86} and Mg/Ca. This is similar to our thermocline/lower mixed-layer foraminifera cooling of ∼1.9 ± 3.5 K (Figure 5) across the EOT.

Our temperature change is also similar in magnitude compared to other calcite-based proxies, such as Mg/Ca from Tanzania (paleolatitude of 16.59°S), which records 0.99 ± 0.37 K cooling (calculated from raw data, study reports ∼2.5 K, Lear et al., 2008) and from ODP sites 738, 744, and 748 (paleolatitude of 56.7°S) with 2.6 K cooling (Bohaty et al., 2012). $\delta^{18}O$-based reconstructions from the Gulf Coast (paleolatitude of 28.5°N) indicate 0.6 K cooling (Kobashi et al., 2004). Note that these $\delta^{18}O_{cc}$-based estimates have a larger uncertainty due to an unknown contribution of potential changes in $\delta^{18}O_{sw}$ to the signal. A clumped-isotope study of Site 689 (paleolatitude of 67.9°S by Petersen and Schrag (2015)) indicated 1.7 ± 4.5 cooling across the EOT. A recent clumped isotope study of the deep Pacific Ocean reconstructed a cooling of 4.7 ± 0.9°C across the EOT (Taylor et al., 2023).

5.3.1. Challenges in Comparing Temperature Reconstructions From Different Proxies

When inferring a latitudinal temperature gradient from specific sites, one needs to take into account potential biases of these site locations with respect to their latitudinal band. Most of the higher-latitude sites are located closer to paleoshorelines, and many of the reconstructions are by necessity derived from semi-enclosed and shallow epeiric seas, potentially leading to warm biases in their SST estimates (Judd et al., 2020) (Figure 1).

As we compare our temperature estimates to those based on different proxies, we briefly discuss the arising challenges. The $U^{k'}_{37}$ data for this interval show strongly fluctuating concentrations of alkenones, often below the required limit (Liu et al., 2018). Low alkenone concentrations have been associated with warm-biases caused by chromatographic irreversible absorption (Grimalt et al., 2001). Many $U^{k'}_{37}$ data also exhibit saturation of the index (Liu et al., 2018), which is thought to occur above 29°C (Brassell et al., 1986). This would, however, result in a bias to cooler than 29°C temperatures. Furthermore, the data in the compilation rely on the Prahl et al. (1988) calibration, which has been shown to have very warm residuals in the North Atlantic (Tierney & Tingley, 2018). This is likely due to sea ice effects and a general summer and fall bias in the North Atlantic on $U^{k'}_{37}$, and while these issues likely did not affect the site to the same extent near the EOT, using these data for the calibration may introduce additional bias.

Some of the challenges with the TEX_{86} proxy are contamination of the target signal with terrestrial inputs of GDGTs, *Euriarchaeota*—which contribute to the GDGT pool through anaerobic oxidation of methane—and, if the *Nitrososphaerota* do contribute significantly to the GDGT pool, potential bias toward summer temperatures. While these issues are largely addressed by the original authors, as well as in later data compilations (Inglis et al., 2015), the production depth of the GDGTs remains disputed. The GDGTs are likely produced in the shallow subsurface (50–300 m) while they were calibrated to the sea surface (see Ho & Laepple, 2016, 2017; Tierney et al., 2017; Tierney, Poulsen, et al., 2020; Zhang & Liu, 2018, for discussion). A potential solution to monitor whether GDGT production occurred at depth has recently been presented in two independent studies (Rattanasriampaipong et al., 2022; van der Weijst et al., 2022), and we will see how this affects future TEX_{86} studies.

The changing Δ_{47} offset that we record between the thermocline/lower mixed-layer dwelling foraminifera and the subthermocline dwelling foraminifera demonstrates that one ought to be careful when using subsurface temperature signals to reconstruct SST. Ocean stratification is spatially heterogeneous and the relationship between the subsurface and the surface, while strong, does not necessarily hold over geologic time and is often variable for modern ocean sites. Production of GDGTs at greater depth may play a small but significant role in the final TEX_{86} signal recorded in the sediment. Therefore it is difficult to assess how the TEX_{86} signal could be affected by changes in stratification through time. Applying a core-top TEX_{86} calibration to modern subsurface temperatures would result in colder reconstructed paleotemperature estimates with smaller variability, which would be in better alignment with model results for latitudinal temperature gradients (Ho & Laepple, 2016). Reconstructing the SST signal from the subsurface by applying a transfer function should be difficult indeed, because we record a changing relationship between the deeper and the shallower water column signals across the EOT.

We do have to consider the potential effects of diagenetic overprinting on our clumped isotope record, as planktonic foraminifera were previously shown to be sensitive to diagenetic overprinting of the $\delta^{18}O$ signal (Pearson et al., 2001; Sexton et al., 2006). However, the foraminifera at the Newfoundland Margin are generally well-preserved (Leutert et al., 2019). We calculated the extent of diagenetic overprinting required to arrive at our

clumped isotope temperatures under several scenarios with set bottom water temperatures and shallow temperatures (further discussed in Text S1 and illustrated in Figure S2 in Supporting Information S1). We find that the worst-case scenario—a warm true formation temperature of ∼20°C with cold bottom water temperatures of 0.0°C for maximum overprinting effect—would require >10 % overprinting, which, from the SEM and light microscope images (Figure 3) and previous studies (Leutert et al., 2019) seems unlikely. Some diagenetic overprinting of the formation temperature cannot be excluded from SEM images alone, and thus our results could be biased toward cooler temperatures captured in the bottom waters and during early diagenesis in the sediment.

After taking into account all of the potential biases above it is hard to elucidate which factors have played a causal role in the discrepancy between the various proxy records, because there are many degrees of freedom to play around with. Overall, we think that our Δ_{47}-based thermocline/lower mixed-layer signal could be compatible with previous organic proxy derived estimates, if those organic proxies would have a shallower origin.

5.4. Lateral Advection

Site U1411 is a sediment drift deposited during the EOT, so temperature reconstructions are likely biased to foraminifera that sank to the North of the site and have been laterally transported (Boyle et al., 2017). Liu et al. (2018) argue why lateral transport of sediments or suspended materials is unlikely to have played a major role for site U1404, which is close to our study Site U1411. First, they note that in the modern ocean there is only an insubstantial difference (∼1.1 K) between alkenone-based temperatures from surface waters and the sea floor in comparison to directly measured SST. Second, that a latitudinal temperature gradient exists for their alkenone-based reconstructions between their site and sites 336 and 913, which are located further North. Third, their reconstructed minimal cooling across the EOT is incompatible with transport from the North, which would occur due to the influence of the deep western boundary current.

Lateral advection in the water column, however, cannot be excluded. It likely influenced how both haptophytic algae and foraminifera were transported to ultimately arrive at the sites. In the middle Eocene (38 Ma) eddying OGCM simulations (Nooteboom et al., 2022) a midlatitude gyre exists, with a northeastward flowing GS. However, the mid-latitude gyre circulates less intensely in these simulations compared to the present-day, likely because the Atlantic basin was more restricted.

The particle advection simulations in the eddying ocean model indicate that the foraminifera were advected by at most 3.3° southward and 2.6° northward near the study site, which indicates that the temperatures they experienced during their lifetime may originate from between 36.2° and 30.5°N and from 39.7° and 29.6°E (transported by 5.3° West or 4.8° East; Figure S11 in Supporting Information S1). In the modern ocean, mixed-layer temperatures 3.3° northwards of Site U1411 are 9.7 K cooler than above Site U1411, while temperatures at 300 m depth are 4.8 K cooler (Locarnini et al., 2019). Even at 300 m depth we see particle transport of more than 4° west during the simulated particles' 30 day life cycle. Furthermore, foraminifera dwelling above site U1404 may end up on Site U1411, and vice-versa (Figures S11 and S13 in Supporting Information S1).

We have to consider that these simulations do not account for foraminifera habitat preferences, however. That is to say, the particle back-track analysis only depends on the ocean currents. In reality, planktonic foraminifera have preferred habitats, such as ranges of temperatures that they can tolerate, as well as for salinity and pH (Nooteboom et al., 2019). For example, it could be that cold eddies from the north are always devoid of foraminifera, and therefore foraminifera-based reconstructions result in a warmer final temperature signal from what is modeled.

On average, however, the particles suspended directly above Site U1411 captured very similar temperatures to those that finally ended up in the sediments of Site U1411 in the simulations. This finding is consistent with temperature reconstructions based on modern and Holocene foraminifera around the site agreeing with observed mixed-layer temperatures. All of our temperature data (Figure 4) are based on many different foraminifera (each datapoint is made up of at least 22 aliquots, each consisting of at least ∼80 µg, so at the very least 100 foraminifera per datapoint), and are thus very likely to capture an average temperature representative of the site's location.

5.5. Increased Ocean Stratification

Our $\delta^{18}O$ and Δ_{47} results show that during the latest Eocene, both thermocline/lower mixed-layer- and subthermocline dwelling foraminifera recorded similar water masses. Toward the Oligocene this changes, with subthermocline dwelling species recording much colder temperatures and higher $\delta^{18}O_{cc}$ values (Figure 4). The

divergence in $\delta^{18}O$ between different planktonic foraminifera species was also found after the EOB in the Gulf of Mexico, which was linked to enhanced seasonality in the earliest Oligocene (Wade et al., 2012).

For Site U1411, this could indicate an adjustment of the growing season of the shallower dwellers or a change in water column stratification. Because at least some of the analyzed foraminifera species occur throughout the record as some of the most abundant species (e.g., *C. unicavus*), we think that the change in recorded thermocline/lower mixed-layer and subthermocline temperature is likely the result of changes in ocean stratification of the upper water column.

5.6. What Could Our Records Mean for AMOC?

The observed changes in North Atlantic stratification may be related to AMOC intensity, which is thought to have initiated or significantly strengthened around 1–0.5 Myr prior to the EOT (i.e., shortly after our oldest datapoint Borrelli et al., 2014; Cramer et al., 2009; Coxall et al., 2018). The onset of the AMOC may be compatible with our record, where we see minor increased stratification prior to the EOT (between our oldest and second-oldest datapoint) with subsequent intensification of the AMOC leading to more pronounced stratification between the subthermocline and the thermocline/lower mixed-layer across the EOT. A model study predicted increased stratification in the North Atlantic, with almost no cooling in the mixed-layer and significant cooling in the thermocline as a result of CO_2 drawdown and subsequent Antarctic Ice Sheet formation (Goldner et al., 2014).

Strengthening (or changes) of bottom water export depth from the North Atlantic is also consistent with seismic stratigraphy, that finds a change in drift sedimentation near the EOT (Boyle et al., 2017). The offset in timing could also be the result of different age models, but this is unlikely around a global event such as the EOT that is marked by large swings in stable isotopes. Changes in AMOC strength have a strong influence on the heat transport in the North Atlantic region. With a stronger AMOC, heat transport intensifies in the mixed-layer via the GS and North Atlantic Drift from the lower latitudes to the higher Northern latitudes. As a consequence of such an AMOC intensification, ocean stratification could have been amplified by increased influence of southern-sourced GS waters on the mixed-layer.

One potential mechanism for the AMOC initiation prior to the EOT was proposed by Hutchinson et al. (2019). They argue that during the late Eocene, some fresh water from the Arctic ocean entered the North Atlantic via the shallow Fram Strait connection. This inflow of low-salinity waters prevented deep-water formation in the North Atlantic. Around the EOT, tectonic closure of the Arctic-Atlantic gateway may have blocked freshwater inflow from the Arctic, resulting in the increased salinity in the North Atlantic and deep water formation at high northern latitudes, leading to AMOC onset or intensification. The warm salt waters from the mid-latitudes were transported farther to the north, warming the region with respect to the Pacific. If restricted to the surface, these warm salty waters could have led to an increased stratification at Site U1411, with a cooler subthermocline than the shallower waters at this site. In the northern North Atlantic, this Arctic-Atlantic gateway closing caused increased mixed-layer depth, but this was limited to areas north of our study site in the model simulation (Hutchinson et al., 2019; Figure S3 in Supporting Information S1). Note that this model study did not include an Antarctic Ice sheet, however, whereas Antarctic Ice Sheet formation has previously been suggested as the driver for AMOC initiation and ocean stratification in the North Atlantic (Goldner et al., 2014).

New data from organic proxies in combination with model simulations demonstrate that the North Atlantic surface ocean could respond strongly to changes in AMOC intensity, which would lead to warming, even if superimposed on a global cooling trend to declining atmospheric CO_2 levels (Śliwińska et al., 2023). This could also explain why, if we look at our four time points separately, it appears that the subthermocline cools first, whereas the thermocline/lower mixed-layer remains warm until shortly prior to the transition. After the EOT, the temperatures align again, potentially indicating a (temporary) interruption of the AMOC. Then, as global cooling continues, thermocline/lower mixed-layer temperatures also drop because the AMOC cannot warm up the mixed-layer at this site more than the global cooling signal. These final points require further investigation, however, because the temperature uncertainties on individual points are relatively large, hampering rigorous statistical analysis.

The observed subthermocline cooling across the EOT can perhaps be ascribed to the global cooling associated with a reduction in atmospheric CO_2, while the thermocline/lower mixed-layer cooling instead is dampened by polar amplification and the intensification of the AMOC across the event, related to Antarctic Ice Sheet formation

(Goldner et al., 2014) or contemporaneous closure of the connection between Arctic and North Atlantic (Hutchinson et al., 2019; Śliwińska et al., 2023).

6. Conclusions

We present the first clumped isotope based upper water column ocean temperatures across the EOT in the North Atlantic region using well-preserved planktonic foraminifera from IODP Site U1411. Earlier studies that have used organic-geochemical proxies to derive SSTs arrive at significantly higher temperatures, which appear inconsistent with modeling simulations. We argue that such differences may originate through various non-thermal influences on the different proxies. Potential biases in the proxy archives are discussed, including the production depth of the signal, seasonality, vital effects, ocean circulation and lateral transport, and diagenesis. We argue that early diagenesis played a minor role in our record and that the discrepancy likely originates from differences in the proxy production depth and/or different seasonal biases.

Our record of both clumped isotopes and stable oxygen isotopes robustly demonstrates a separation of thermocline/lower mixed-layer dwelling from subthermocline dwelling foraminifera, indicating changing ocean stratification, potentially associated with the increased AMOC strength. Importantly, we find a larger cooling in the subthermocline compared to the thermocline/lower mixed-layer reconstructions in both $\delta^{18}O_{cc}$ and Δ_{47}, which is consistent with a scenario in which global cooling associated with a drop in atmospheric CO_2 is accompanied by an onset of the AMOC due to Antarctic Ice Sheet formation and/or tectonic restrictions in the connections between the Arctic and the North Atlantic. This increased stratification further highlights the potential caveats of calibrating proxy records to SST, if the depth of production of the carrier signal is not well-known. Future research on ocean stratification and the development of the AMOC could benefit from more multiproxy reconstructions for this region, hopefully elucidating causes of the discrepancies we observe between proxy records.

Data Availability Statement

The code used to read mass spectrometer data from machine output is available on https://github.com/isoverse/isoreader (Kopf et al., 2021). Code to process these to final clumped values is distributed under the GPL-3 license and is available in Kocken (2019). The UU-specific processing code is available in Kocken (2022). The code used to apply a bootstrapped York regression to a calibration data set and apply this in combination with the $\delta^{18}O_{sw}$ calculation is available via Kocken (2023), also under the GPL-3 license. All clumped isotope replicate data have been uploaded to the EarthChem database, available on Kocken et al. (2024). The code used for the back-tracking analysis is distributed under the MIT license and can be found at Nooteboom (2023). Model output and boundary conditions such as the bathymetry can be found on YODA via Nooteboom (2022).

Acknowledgments
IJK acknowledges Arnold van Dijk for laboratory assistance. This work is part of the NWO Vidi project 016.161.365, which is financed by the Netherlands Organization for Scientific Research (NWO). Analyses at the UiB were possible through funding from the Bjerknes Centre for Climate Research through a fast track initiative grant to Petra Langebroek. PN acknowledges support from the Netherlands Organization for Scientific Research (NWO), Earth and Life Sciences, through project ALWOP.207. The use of the SURFsara computing facilities was sponsored by NWO-EW (Netherlands Organization for Scientific Research, Exact Sciences) under the project 15508. ANM acknowledges funding from the European Research Council (project number 638467). We thank reviewers for providing constructive feedback that has greatly improved the manuscript.

References

Anderson, N. T., Kelson, J. R., Kele, S., Daëron, M., Bonifacie, M., Horita, J., et al. (2021). A unified clumped isotope thermometer calibration (0.5–1100°C) using carbonate-based standardization. *Geophysical Research Letters*, *48*(7), e2020GL092069. https://doi.org/10.1029/2020GL092069

Armstrong McKay, D. I., Tyrrell, T., & Wilson, P. A. (2016). Global carbon cycle perturbation across the Eocene-Oligocene climate transition. *Paleoceanography*, *31*(2), 311–329. https://doi.org/10.1002/2015PA002818

Baatsen, M., van Hinsbergen, D. J. J., von der Heydt, A. S., Dijkstra, H. A., Sluijs, A., Abels, H. A., & Bijl, P. K. (2016). Reconstructing geographical boundary conditions for palaeoclimate modelling during the Cenozoic. *Climate of the Past*, *12*(8), 1635–1644. https://doi.org/10.5194/cp-12-1635-2016

Bemis, B. E., Spero, H. J., Bijma, J., & Lea, D. W. (1998). Reevaluation of the oxygen isotopic composition of planktonic foraminifera: Experimental results and revised paleotemperature equations. *Paleoceanography*, *13*(2), 150–160. https://doi.org/10.1029/98PA00070

Bernasconi, S. M., Daëron, M., Bergmann, K. D., Bonifacie, M., Meckler, A. N., Affek, H. P., et al. (2021). InterCarb: A community effort to improve inter-laboratory standardization of the carbonate clumped isotope thermometer using carbonate standards. *Geochemistry, Geophysics, Geosystems*, *22*(5), e2020GC009588. https://doi.org/10.1029/2020GC009588

Bernasconi, S. M., Hu, B., Wacker, U., Fiebig, J., Breitenbach, S. F. M., & Rutz, T. (2013). Background effects on Faraday collectors in gas-source mass spectrometry and implications for clumped isotope measurements. *Rapid Communications in Mass Spectrometry*, *27*(5), 603–612. https://doi.org/10.1002/rcm.6490

Bernasconi, S. M., Müller, I. A., Bergmann, K. D., Breitenbach, S. F. M., Fernandez, A., Hodell, D. A., et al. (2018). Reducing uncertainties in carbonate clumped isotope analysis through consistent carbonate-based standardization. *Geochemistry, Geophysics, Geosystems*, *19*(9), 2895–2914. https://doi.org/10.1029/2017GC007385

Boersma, A., Silva, I. P., & Shackleton, N. J. (1987). Atlantic Eocene planktonic foraminiferal paleohydrographic indicators and stable isotope paleoceanography. *Paleoceanography*, *2*(3), 287–331. https://doi.org/10.1029/PA002i003p00287

Bohaty, S. M., Zachos, J. C., & Delaney, M. L. (2012). Foraminiferal Mg/Ca evidence for Southern Ocean cooling across the Eocene–Oligocene transition. *Earth and Planetary Science Letters*, *317–318*, 251–261. https://doi.org/10.1016/j.epsl.2011.11.037

Borrelli, C., Cramer, B. S., & Katz, M. E. (2014). Bipolar Atlantic deepwater circulation in the middle-late Eocene: Effects of Southern Ocean gateway openings. *Paleoceanography*, *29*(4), 308–327. https://doi.org/10.1002/2012PA002444

Boyle, P. R., Romans, B. W., Tucholke, B. E., Norris, R. D., Swift, S. A., & Sexton, P. F. (2017). Cenozoic North Atlantic deep circulation history recorded in contourite drifts, offshore Newfoundland, Canada. *Marine Geology*, *385*, 185–203. https://doi.org/10.1016/j.margeo.2016.12.014

Brassell, S. C., Eglinton, G., Marlowe, I. T., Pflaumann, U., & Sarnthein, M. (1986). Molecular stratigraphy: A new tool for climatic assessment. *Nature*, *320*(6058), 129–133. https://doi.org/10.1038/320129a0

Cléroux, C., Cortijo, E., Anand, P., Labeyrie, L. D., Bassinot, F. C., Caillon, N., & Duplessy, J.-C. (2008). Mg/Ca and Sr/Ca ratios of planktonic foraminifera from North Atlantic surface sediments. *PANGAEA*. https://doi.org/10.1594/PANGAEA.832178

Coxall, H. K., Huck, C. E., Huber, M., Lear, C. H., Legarda-Lisarri, A., O'Regan, M., et al. (2018). Export of nutrient rich northern component water preceded early Oligocene Antarctic glaciation. *Nature Geoscience*, *11*(3), 190–196. https://doi.org/10.1038/s41561-018-0069-9

Coxall, H. K., Jones, T. D., Jones, A. P., Lunt, P., MacMillan, I., Marliyani, G. I., et al. (2021). The Eocene-Oligocene transition in Nanggulan, Java: Lithostratigraphy, biostratigraphy and foraminiferal stable isotopes. *Journal of the Geological Society*, *178*(6), jgs2021-006. https://doi.org/10.1144/jgs2021-006

Coxall, H. K., & Pearson, P. (2007). The Eocene–Oligocene transition. In M. Williams, A. Haywood, F. Gregory, & D. Schmidt (Eds.), *Deep-time perspectives on climate change: Marrying the signal from computer models and biological proxies* (1st ed., pp. 351–387). The Geological Society of London on behalf of The Micropalaeontological Society. https://doi.org/10.1144/TMS002.16

Coxall, H. K., & Spezzaferri, S. (2018). Taxonomy, biostratigraphy, and, phylogeny of Oligocene *Catapsydrax*, *Globorotaloides* and *Protentelloides*. *Cushman Foundation Special Publication*, *4*(46), 79–124.

Cramer, B. S., Toggweiler, J. R., Wright, J. D., Katz, M. E., & Miller, K. G. (2009). Ocean overturning since the late cretaceous: Inferences from a new benthic foraminiferal isotope compilation. *Paleoceanography*, *24*(4), 1–14. https://doi.org/10.1029/2008PA001683

Dennis, K. J., Affek, H. P., Passey, B. H., Schrag, D. P., & Eiler, J. M. (2011). Defining an absolute reference frame for 'clumped' isotope studies of CO_2. *Geochimica et Cosmochimica Acta*, *75*(22), 7117–7131. https://doi.org/10.1016/j.gca.2011.09.025

De Schepper, S., Groeneveld, J., Naafs, B. D. A., Van Renterghem, C., Hennissen, J., Head, M. J., et al. (2013). Northern hemisphere glaciation during the globally warm Early Late Pliocene. *PLoS One*, *8*(12), e81508. https://doi.org/10.1371/journal.pone.0081508

Elsworth, G., Galbraith, E., Halverson, G., & Yang, S. (2017). Enhanced weathering and CO_2 drawdown caused by latest Eocene strengthening of the Atlantic meridional overturning circulation. *Nature Geoscience*, *10*(3), 213–216. https://doi.org/10.1038/ngeo2888

Erez, J., & Luz, B. (1983). Experimental paleotemperature equation for planktonic foraminifera. *Geochimica et Cosmochimica Acta*, *47*(6), 1025–1031. https://doi.org/10.1016/0016-7037(83)90232-6

Ganssen, G. M., & Kroon, D. (2000). The isotopic signature of planktonic foraminifera from NE Atlantic surface sediments: Implications for the reconstruction of past oceanic conditions. *Journal of the Geological Society*, *157*(3), 693–699. https://doi.org/10.1144/jgs.157.3.693

Goldner, A., Herold, N., & Huber, M. (2014). Antarctic glaciation caused ocean circulation changes at the Eocene–Oligocene transition. *Nature*, *511*(7511), 574–577. https://doi.org/10.1038/nature13597

Grimalt, J. O., Calvo, E., & Pelejero, C. (2001). Sea surface paleotemperature errors in $U_{37}^{K'}$ estimation due to alkenone measurements near the limit of detection. *Paleoceanography*, *16*(2), 226–232. https://doi.org/10.1029/1999PA000440

Groeneveld, J., & Chiessi, C. M. (2011). Mg/Ca of Globorotalia inflata as a recorder of permanent thermocline temperatures in the South Atlantic. *Paleoceanography*, *26*(2), PA2203. https://doi.org/10.1029/2010PA001940

He, B., Olack, G. A., & Colman, A. S. (2012). Pressure baseline correction and high-precision CO_2 clumped-isotope (Δ_{47}) measurements in bellows and micro-volume modes. *Rapid Communications in Mass Spectrometry*, *26*(24), 2837–2853. https://doi.org/10.1002/rcm.6436

Ho, S. L., & Laepple, T. (2016). Flat meridional temperature gradient in the early Eocene in the subsurface rather than surface ocean. *Nature Geoscience*, *9*(8), 606–610. https://doi.org/10.1038/ngeo2763

Ho, S. L., & Laepple, T. (2017). Reply to 'Eocene temperature gradients'. *Nature Geoscience*, *10*(8), 539–540. https://doi.org/10.1038/ngeo2998

Hollis, C. J., Dunkley Jones, T., Anagnostou, E., Bijl, P. K., Cramwinckel, M. J., Cui, Y., et al. (2019). The DeepMIP contribution to PMIP4: Methodologies for selection, compilation and analysis of latest Paleocene and early Eocene climate proxy data, incorporating version 0.1 of the DeepMIP database. *Geoscientific Model Development*, *12*(7), 3149–3206. https://doi.org/10.5194/gmd-12-3149-2019

Holmström, M. (2016). *Planktonic foraminifera biostratigraphy and assemblage analysis across the Eocene/Oligocene boundary at IODP Site U1411, Newfoundland Margin (MSc)*. Stockholm University.

Hu, B., Radke, J., Schlüter, H. J., Heine, F. T., Zhou, L., & Bernasconi, S. M. (2014). A modified procedure for gas-source isotope ratio mass spectrometry: The long-integration dual-inlet (LIDI) methodology and implications for clumped isotope measurements. *Rapid Communications in Mass Spectrometry*, *28*(13), 1413–1425. https://doi.org/10.1002/rcm.6909

Huber, B., Petrizzo, M., Young, J., Falzoni, F., Gilardoni, S., Bown, P., & Wade, B. (2016). Pforams@microtax: A new online taxonomic database for planktonic foraminifera. *Micropaleontology*, *62*(6), 429–438. https://doi.org/10.47894/mpal.62.6.02

Huber, M., & Caballero, R. (2011). The early Eocene equable climate problem revisited. *Climate of the Past*, *7*(2), 603–633. https://doi.org/10.5194/cp-7-603-2011

Hutchinson, D. K., Coxall, H. K., Lunt, D. J., Steinthorsdottir, M., de Boer, A. M., Baatsen, M., et al. (2021). The Eocene–Oligocene transition: A review of marine and terrestrial proxy data, models and model–data comparisons. *Climate of the Past*, *17*(1), 269–315. https://doi.org/10.5194/cp-17-269-2021

Hutchinson, D. K., Coxall, H. K., O'Regan, M., Nilsson, J., Caballero, R., & de Boer, A. M. (2019). Arctic closure as a trigger for Atlantic overturning at the Eocene-Oligocene transition. *Nature Communications*, *10*(1), 3797. https://doi.org/10.1038/s41467-019-11828-z

Hutchinson, D. K., de Boer, A. M., Coxall, H. K., Caballero, R., Nilsson, J., & Baatsen, M. (2018). Climate sensitivity and meridional overturning circulation in the late Eocene using GFDL CM2.1. *Climate of the Past*, *14*(6), 789–810. https://doi.org/10.5194/cp-14-789-2018

Inglis, G. N., Farnsworth, A., Lunt, D., Foster, G. L., Hollis, C. J., Pagani, M., et al. (2015). Descent toward the Icehouse: Eocene sea surface cooling inferred from GDGT distributions. *Paleoceanography*, *30*(7), 1000–1020. https://doi.org/10.1002/2014PA002723

Inkscape Project. (2021). Inkscape. Retrieved from https://inkscape.org

Judd, E. J., Bhattacharya, T., & Ivany, L. C. (2020). A dynamical framework for interpreting ancient sea surface temperatures. *Geophysical Research Letters*, *47*(15), e2020GL089044. https://doi.org/10.1029/2020GL089044

Kaminski, M. A., & Ortiz, S. (2014). The Eocene-Oligocene turnover of deep-water agglutinated foraminifera at ODP site 647, southern Labrador Sea (North Atlantic). *Micropaleontology*, *60*(1), 53–66. https://doi.org/10.47894/mpal.60.1.06

Kim, S.-T., & O'Neil, J. R. (1997). Equilibrium and nonequilibrium oxygen isotope effects in synthetic carbonates. *Geochimica et Cosmochimica Acta*, *61*(16), 3461–3475. https://doi.org/10.1016/S0016-7037(97)00169-5

Kobashi, T., Grossman, E. L., Dockery, D. T., III, & Ivany, L. C. (2004). Water mass stability reconstructions from greenhouse (Eocene) to icehouse (Oligocene) for the northern Gulf Coast continental shelf (USA). *Paleoceanography and Paleoclimatology*, *19*(1), PA1022. https://doi.org/10.1029/2003PA000934

Kocken, I. J. (2019). clumpedr: Clumped isotope processing in R (v0.2.0) [Software]. *Zenodo*. https://doi.org/10.5281/zenodo.10638817
Kocken, I. J. (2022). clumped-processing: R scripts to process clumped isotopes from raw data to final values at Utrecht Univerity (v1.0.0) [Software]. *Zenodo*. https://doi.org/10.5281/zenodo.6421836
Kocken, I. J. (2023). clumpedcalib: Calculate and apply clumped isotope calibrations using bootstrapping (v0.0.2) [Software]. *Zenodo*. https://doi.org/10.5281/zenodo.8148801
Kocken, I. J., Müller, I. A., & Ziegler, M. (2019). Optimizing the use of carbonate standards to minimize uncertainties in clumped isotope data. *Geochemistry, Geophysics, Geosystems*, *20*(11), 5565–5577. https://doi.org/10.1029/2019GC008545
Kocken, I. J., Nooteboom, P. D., van der Veen, K., Coxall, H. K., Müller, I. A., Meckler, A. N., & Ziegler, M. (2024). Clumped isotope data for North Atlantic temperature change across the Eocene–Oligocene transition (1.0) [Dataset]. *Interdisciplinary Earth Data Alliance (IEDA)*. https://doi.org/10.60520/IEDA/112998
Kopf, S., Davidheiser-Kroll, B., & Kocken, I. J. (2021). Isoreader: An R package to read stable isotope data files for reproducible research. *JOSS*, *6*(61), 2878. https://doi.org/10.21105/joss.02878
Kucera, M. (2007). Chapter six planktonic foraminifera as tracers of past oceanic environments. In C. Hillaire-Marcel & A. De Vernal (Eds.), *Developments in marine Geology* (Vol. 1, pp. 213–262). Elsevier. https://doi.org/10.1016/S1572-5480(07)01011-1
Lear, C. H., Bailey, T. R., Pearson, P. N., Coxall, H. K., & Rosenthal, Y. (2008). Cooling and ice growth across the Eocene-Oligocene transition. *Geology*, *36*(3), 251–254. https://doi.org/10.1130/G24584A.1
Leutert, T. J., Sexton, P. F., Tripati, A., Piasecki, A., Ho, S. L., & Meckler, A. N. (2019). Sensitivity of clumped isotope temperatures in fossil benthic and planktic foraminifera to diagenetic alteration. *Geochimica et Cosmochimica Acta*, *257*, 354–372. https://doi.org/10.1016/j.gca.2019.05.005
Liu, Z., He, Y., Jiang, Y., Wang, H., Liu, W., Bohaty, S. M., & Wilson, P. A. (2018). Transient temperature asymmetry between hemispheres in the Palaeogene Atlantic Ocean. *Nature Geoscience*, *11*(9), 656–660. https://doi.org/10.1038/s41561-018-0182-9
Liu, Z., Pagani, M., Zinniker, D., DeConto, R., Huber, M., Brinkhuis, H., et al. (2009). Global cooling during the Eocene–Oligocene climate transition. *Science*, *323*(5918), 1187–1190. https://doi.org/10.1126/science.1166368
Locarnini, R. A., Baranova, O. K., Mishonov, A. V., Boyer, T. P., Reagan, J. R., Dukhovskoy, D., et al. (2023). *World Ocean Atlas 2023, volume 1: Temperature (technical report)*. NOAA. Retrieved from https://www.ncei.noaa.gov/access/world-ocean-atlas-2023/bin/woa23.pl
Locarnini, R. A., Mishonov, A. V., Baranova, O. K., Boyer, T. P., Zweng, M. M., Garcia, H. E., et al. (2019). *World Ocean Atlas 2018, volume 1: Temperature (technical report)*. NOAA.
Marchitto, T. M., Curry, W. B., Lynch-Stieglitz, J., Bryan, S. P., Cobb, K. M., & Lund, D. C. (2014). Improved oxygen isotope temperature calibrations for cosmopolitan benthic foraminifera. *Geochimica et Cosmochimica Acta*, *130*, 1–11. https://doi.org/10.1016/j.gca.2013.12.034
Marzocchi, A., Hirschi, J. J. M., Holliday, N. P., Cunningham, S. A., Blaker, A. T., & Coward, A. C. (2015). The North Atlantic subpolar circulation in an eddy-resolving global ocean model. *Journal of Marine Systems*, *142*, 126–143. https://doi.org/10.1016/j.jmarsys.2014.10.007
Meckler, A. N., Ziegler, M., Millán, M. I., Breitenbach, S. F. M., & Bernasconi, S. M. (2014). Long-term performance of the Kiel carbonate device with a new correction scheme for clumped isotope measurements: Performance and correction of Kiel clumped isotope measurements. *Rapid Communications in Mass Spectrometry*, *28*(15), 1705–1715. https://doi.org/10.1002/rcm.6949
Meinicke, N., Ho, S. L., Hannisdal, B., Nürnberg, D., Tripati, A. K., Schiebel, R., & Meckler, A. N. (2020). A robust calibration of the clumped isotopes to temperature relationship for foraminifers. *Geochimica et Cosmochimica Acta*, *270*, 160–183. https://doi.org/10.1016/j.gca.2019.11.022
Meinicke, N., Reimi, M. A., Ravelo, A. C., & Meckler, A. N. (2021). Coupled Mg/Ca and clumped isotope measurements indicate lack of substantial mixed layer cooling in the Western Pacific Warm Pool during the last ~5 million years. *Paleoceanography and Paleoclimatology*, *36*(8), e2020PA004115. https://doi.org/10.1029/2020PA004115
Moore, T. C., Jr., Wade, B. S., Westerhold, T., Erhardt, A. M., Coxall, H. K., Baldauf, J., & Wagner, M. (2014). Equatorial Pacific productivity changes near the Eocene-Oligocene boundary. *Paleoceanography*, *29*(9), 825–844. https://doi.org/10.1002/2014PA002656
Müller, I. A., Fernandez, A., Radke, J., van Dijk, J., Bowen, D., Schwieters, J., & Bernasconi, S. M. (2017). Carbonate clumped isotope analyses with the long-integration dual-inlet (LIDI) workflow: Scratching at the lower sample weight boundaries. *Rapid Communications in Mass Spectrometry*, *31*(12), 1057–1066. https://doi.org/10.1002/rcm.7878
Müller, I. A., Violay, M. E. S., Storck, J.-C., Fernandez, A., van Dijk, J., Madonna, C., & Bernasconi, S. M. (2017). Clumped isotope fractionation during phosphoric acid digestion of carbonates at 70°C. *Chemical Geology*, *449*, 1–14. https://doi.org/10.1016/j.chemgeo.2016.11.030
Müller, R. D., Cannon, J., Qin, X., Watson, R. J., Gurnis, M., Williams, S., et al. (2018). GPlates: Building a virtual earth through deep time. *Geochemistry, Geophysics, Geosystems*, *19*(7), 2243–2261. https://doi.org/10.1029/2018GC007584
Nooteboom, P. D. (2022). POP data for Nooteboom et al., 2022 [Dataset]. *Yoda Utrecht University*. https://doi.org/10.24416/UU01-9NFEKH
Nooteboom, P. D. (2023). pdnooteboom/NA_forams: Code for 'North Atlantic temperature change across the Eocene–Oligocene Transition' (v1) [Software]. *Zenodo*. https://doi.org/10.5281/ZENODO.10148207
Nooteboom, P. D., Baatsen, M., Bijl, P. K., Kliphuis, M. A., van Sebille, E., Sluijs, A., et al. (2022). Improved model-data agreement with strongly eddying ocean simulations in the middle–late Eocene. *Paleoceanography and Paleoclimatology*, *37*(8), e2021PA004405. https://doi.org/10.1029/2021PA004405
Nooteboom, P. D., Bijl, P. K., van Sebille, E., von der Heydt, A. S., & Dijkstra, H. A. (2019). Transport bias by ocean currents in sedimentary microplankton assemblages: Implications for paleoceanographic reconstructions. *Paleoceanography and Paleoclimatology*, *34*(7), 1178–1194. https://doi.org/10.1029/2019PA003606
Nooteboom, P. D., Delandmeter, P., van Sebille, E., Bijl, P. K., Dijkstra, H. A., & von der Heydt, A. S. (2020). Resolution dependency of sinking Lagrangian particles in ocean general circulation models. *PLoS One*, *15*(9), e0238650. https://doi.org/10.1371/journal.pone.0238650
Norris, R. D., Wilson, P. A., Blum, P., Fehr, A., Agnini, C., Bornemann, A., et al. (Eds.) (2014). *Expedition 342 summary (No. 342)*. Integrated Ocean Drilling Program. https://doi.org/10.2204/iodp.proc.342.2014
Pearson, P. N., Ditchfield, P. W., Singano, J., Harcourt-Brown, K. G., Nicholas, C. J., Olsson, R. K., et al. (2001). Warm tropical sea surface temperatures in the Late Cretaceous and Eocene epochs. *Nature*, *413*(6855), 481–487. https://doi.org/10.1038/35097000
Pearson, P. N., McMillan, I. K., Wade, B. S., Jones, T. D., Coxall, H. K., Bown, P. R., & Lear, C. H. (2008). Extinction and environmental change across the Eocene-Oligocene boundary in Tanzania. *Geology*, *36*(2), 179–182. https://doi.org/10.1130/G24308A.1
Pearson, P. N., Olsson, R. K., Spezzaferri, S., & Leckie, R. M. (2018). Taxonomy, biostratigraphy, and phylogeny of Oligocene *Globanomalinidae* (*Pseudohastigerina* and *Turborotalia*). In *Atlas of Oligocene planktonic foraminifera*. Cushman Foundation for Foraminiferal Research. Retrieved from https://pubs.geoscienceworld.org/cushmanfoundation/books/book/2271/chapter/126275381
Pearson, P. N., Premec-Fucek, V., & Silva, I. P. (2006). Taxonomy, biostratigraphy, and phylogeny of Eocene *Turborotalia*. Atlas of Eocene planktonic foraminifera. *Cushman Foundation Special Publication*, *41*, 433–460.

Pearson, P. N., van Dongen, B. E., Nicholas, C. J., Pancost, R. D., Schouten, S., Singano, J. M., & Wade, B. S. (2007). Stable warm tropical climate through the Eocene Epoch. *Geology*, *35*(3), 211–214. https://doi.org/10.1130/G23175A.1

Pearson, P. N., & Wade, B. S. (2015). *Systematic taxonomy of exceptionally well-preserved planktonic foraminifera from the Eocene/Oligocene boundary of Tanzania* (pp. 1–85). Special Publication 45: Cushman Foundation for Foraminiferal Research. Retrieved from http://www.cushmanfoundation.org/specpubs/sp45.php

Peral, M., Bassinot, F., Daëron, M., Blamart, D., Bonnin, J., Jorissen, F., et al. (2022). On the combination of the planktonic foraminiferal Mg/Ca, clumped (Δ_{47}) and conventional ($\delta^{18}O$) stable isotope paleothermometers in palaeoceanographic studies. *Geochimica et Cosmochimica Acta*, *339*, 22–34. https://doi.org/10.1016/j.gca.2022.10.030

Peral, M., Daëron, M., Blamart, D., Bassinot, F., Dewilde, F., Smialkowski, N., et al. (2018). Updated calibration of the clumped isotope thermometer in planktonic and benthic foraminifera. *Geochimica et Cosmochimica Acta*, *239*, 1–16. https://doi.org/10.1016/j.gca.2018.07.016

Petersen, S. V., & Schrag, D. P. (2015). Antarctic ice growth before and after the Eocene-Oligocene transition: New estimates from clumped isotope paleothermometry. *Paleoceanography*, *30*(10), 1305–1317. https://doi.org/10.1002/2014PA002769

Piga, E. (2020). *How hot is hot? Tropical ocean temperatures and plankton communities in the Eocene Epoch (Doctoral dissertation)*. Cardiff University. Retrieved from http://orca.cf.ac.uk/136990/

Porta Mana, P., & Zanna, L. (2014). Toward a stochastic parameterization of ocean mesoscale eddies. *Ocean Modelling*, *79*, 1–20. https://doi.org/10.1016/j.ocemod.2014.04.002

Prahl, F. G., Muehlhausen, L. A., & Zahnle, D. L. (1988). Further evaluation of long-chain alkenones as indicators of paleoceanographic conditions. *Geochimica et Cosmochimica Acta*, *52*(9), 2303–2310. https://doi.org/10.1016/0016-7037(88)90132-9

Rattanasriampaipong, R., Zhang, Y. G., Pearson, A., Hedlund, B. P., & Zhang, S. (2022). Archaeal lipids trace ecology and evolution of marine ammonia-oxidizing archaea. *Proceedings of the National Academy of Sciences*, *119*(31), e2123193119. https://doi.org/10.1073/pnas.2123193119

R Core Team. (2020). *R: A language and environment for statistical computing*. R Foundation for Statistical Computing. Retrieved from https://www.R-project.org/

Rebotim, A., Voelker, A., Jonkers, L., Waniek, J. J., Meggers, H., Schiebel, R., et al. (2017). Factors controlling the depth habitat of planktonic foraminifera in the subtropical eastern North Atlantic. *Biogeosciences*, *14*(4), 827–859. https://doi.org/10.5194/bg-14-827-2017

Regenberg, M., Regenberg, A., Garbe-Schönberg, D., & Lea, D. W. (2014). Global dissolution effects on planktonic foraminiferal Mg/Ca ratios controlled by the calcite-saturation state of bottom waters. *Paleoceanography*, *29*(3), 127–142. https://doi.org/10.1002/2013PA002492

Renaudie, J., Lazarus, D. B., & Diver, P. (2020). NSB (Neptune Sandbox Berlin): An expanded and improved database of marine planktonic microfossil data and deep-sea stratigraphy. *Palaeontologia Electronica*, *23*(1), 1–28. https://doi.org/10.26879/1032

Riveiros, N. V., Govin, A., Waelbroeck, C., Mackensen, A., Michel, E., Moreira, S., et al. (2016). Mg/Ca thermometry in planktic foraminifera: Improving paleotemperature estimations for *G. bulloides* and *N. pachyderma* left. *Geochemistry, Geophysics, Geosystems*, *17*(4), 1249–1264. https://doi.org/10.1002/2015GC006234

Schmid, T. W., & Bernasconi, S. M. (2010). An automated method for 'clumped-isotope' measurements on small carbonate samples. *Rapid Communications in Mass Spectrometry*, *24*(14), 1955–1963. https://doi.org/10.1002/rcm.4598

Schmidt, G. A., Bigg, G. R., & Rohling, E. J. (1999). Global seawater oxygen-18 database - v1.22. Retrieved from https://data.giss.nasa.gov/o18data/

Sexton, P. F., & Wilson, P. A. (2009). Preservation of benthic foraminifera and reliability of deep-sea temperature records: Importance of sedimentation rates, lithology, and the need to examine test wall structure. *Paleoceanography*, *24*(2), 1–14. https://doi.org/10.1029/2008PA001650

Sexton, P. F., Wilson, P. A., & Pearson, P. N. (2006). Microstructural and geochemical perspectives on planktic foraminiferal preservation: "Glassy" versus "frosty". *Geochemistry, Geophysics, Geosystems*, *7*(12), Q12P19. https://doi.org/10.1029/2006GC001291

Shackleton, N. J. (1974). Attainment of isotopic equilibrium between ocean water and the benthic foraminifera genus Uvigerina: Isotopic changes in the ocean during the last glacial. *Colloques Internationaux du CNRS*, *219*, 203–209.

Śliwińska, K. K., Coxall, H. K., Hutchinson, D. K., Liebrand, D., Schouten, S., & de Boer, A. M. (2023). Sea surface temperature evolution of the North Atlantic Ocean across the Eocene–Oligocene transition. *Climate of the Past*, *19*(1), 123–140. https://doi.org/10.5194/cp-19-123-2023

Śliwińska, K. K., Thomsen, E., Schouten, S., Schoon, P. L., & Heilmann-Clausen, C. (2019). Climate- and gateway-driven cooling of late Eocene to earliest Oligocene sea surface temperatures in the North Sea Basin. *Scientific Reports*, *9*(1), 4458. https://doi.org/10.1038/s41598-019-41013-7

Speijer, R. P., Pälike, H., Hollis, C. J., Hooker, J. J., & Ogg, J. G. (2020). Chapter 28—The Paleogene period. In F. M. Gradstein, J. G. Ogg, M. D. Schmitz, & G. M. Ogg (Eds.), *Geologic time scale 2020* (pp. 1087–1140). Elsevier. https://doi.org/10.1016/B978-0-12-824360-2.00028-0

Stärz, M., Jokat, W., Knorr, G., & Lohmann, G. (2017). Threshold in North Atlantic-Arctic ocean circulation controlled by the subsidence of the Greenland-Scotland Ridge. *Nature Communications*, *8*(1), 15681. https://doi.org/10.1038/ncomms15681

Straume, E. O., Nummelin, A., Gaina, C., & Nisancioglu, K. H. (2022). Climate transition at the Eocene–Oligocene influenced by bathymetric changes to the Atlantic–Arctic oceanic gateways. *Proceedings of the National Academy of Sciences*, *119*(17), e2115346119. https://doi.org/10.1073/pnas.2115346119

Takahashi, K., & Be, A. W. (1984). Planktonic foraminifera: Factors controlling sinking speeds. Deep Sea Research Part A. *Oceanographic Research Papers*, *31*(12), 1477–1500. https://doi.org/10.1016/0198-0149(84)90083-9

Taylor, V. E., Wilson, P. A., Bohaty, S. M., & Meckler, A. N. (2023). Transient deep ocean cooling in the eastern equatorial Pacific Ocean at the Eocene-Oligocene transition. *Paleoceanography and Paleoclimatology*, *38*(8), e2023PA004650. https://doi.org/10.1029/2023PA004650

Tierney, J. E., Poulsen, C. J., Montañez, I. P., Bhattacharya, T., Feng, R., Ford, H. L., et al. (2020). Past climates inform our future. *Science*, *370*(6517), eaay3701. https://doi.org/10.1126/science.aay3701

Tierney, J. E., Sinninghe Damsté, J. S., Pancost, R. D., Sluijs, A., & Zachos, J. C. (2017). Eocene temperature gradients. *Nature Geoscience*, *10*(8), 538–539. https://doi.org/10.1038/ngeo2997

Tierney, J. E., & Tingley, M. P. (2018). BAYSPLINE: A new calibration for the alkenone paleothermometer. *Paleoceanography and Paleoclimatology*, *33*(3), 281–301. https://doi.org/10.1002/2017PA003201

Tierney, J. E., Zhu, J., King, J., Malevich, S. B., Hakim, G. J., & Poulsen, C. J. (2020). Glacial cooling and climate sensitivity revisited. *Nature*, *584*(7822), 569–573. https://doi.org/10.1038/s41586-020-2617-x

Tolderlund, D. S., Bé, A. W. H., & Be, A. W. H. (1971). Seasonal distribution of planktonic foraminifera in the western North Atlantic. *Micropaleontology*, *17*(3), 297–329. https://doi.org/10.2307/1485143

Torsvik, T. H., van der Voo, R., Preeden, U., Niocaill, C. M., Steinberger, B., Doubrovine, P. V., et al. (2012). Phanerozoic polar wander, palaeogeography and dynamics. *Earth-Science Reviews*, *114*(3–4), 325–368. https://doi.org/10.1016/j.earscirev.2012.06.002

van der Weijst, C. M. H., van der Laan, K. J., Peterse, F., Reichart, G.-J., Sangiorgi, F., Schouten, S., et al. (2022). A 15-million-year surface- and subsurface-integrated TEX_{86} temperature record from the eastern equatorial Atlantic. *Climate of the Past*, *18*(8), 1947–1962. https://doi.org/10.5194/cp-18-1947-2022

van Hinsbergen, D. J. J., de Groot, L. V., van Schaik, S. J., Spakman, W., Bijl, P. K., Sluijs, A., et al. (2015). A paleolatitude calculator for paleoclimate studies. *PLoS One*, *10*(6), e0126946. https://doi.org/10.1371/journal.pone.0126946

van Sebille, E., Scussolini, P., Durgadoo, J. V., Peeters, F. J. C., Biastoch, A., Weijer, W., et al. (2015). Ocean currents generate large footprints in marine palaeoclimate proxies. *Nature Communications*, *6*(1), 6521. https://doi.org/10.1038/ncomms7521

Wade, B. S., Houben, A. J. P., Quaijtaal, W., Schouten, S., Rosenthal, Y., Miller, K. G., et al. (2012). Multiproxy record of abrupt sea-surface cooling across the Eocene-Oligocene transition in the Gulf of Mexico. *Geology*, *40*(2), 159–162. https://doi.org/10.1130/G32577.1

Wade, B. S., Olsson, R. K., Pearson, P. N., Edgar, K. M., Premoli Silva, I., Wade, B. S., et al. (2018). Taxonomy, biostratigraphy, and phylogeny of Oligocene *Subbotina*. In *Atlas of Oligocene planktonic foraminifera* (Vol. 46, pp. 307–330). Cushman Foundation for Foraminiferal Research. Retrieved from https://pubs.geoscienceworld.org/cushmanfoundation/books/book/2271/chapter-abstract/126275363

Wade, B. S., Olsson, R. K., Pearson, P. N., Huber, B. T., & Berggren, W. A. (2018). *Atlas of Oligocene planktonic foraminifera* (Vol. 46). Cushman Foundation for Foraminiferal Research. Retrieved from https://pubs.geoscienceworld.org/cushmanfoundation/books/book/2271

Wade, B. S., & Pearson, P. N. (2008). Planktonic foraminiferal turnover, diversity fluctuations and geochemical signals across the Eocene/Oligocene boundary in Tanzania. *Marine Micropaleontology*, *68*(3), 244–255. https://doi.org/10.1016/j.marmicro.2008.04.002

Wade, B. S., Pearson, P. N., Olsson, R. K., Fraass, A. J., Leckie, M., & Hemleben, C. (2018). Taxonomy, biostratigraphy, and phylogeny of Oligocene and lower Miocene *Dentoglobigerina* and *Globoquadrina*. In *Atlas of Oligocene planktonic foraminifera* (Vol. 46, pp. 331–384). Cushman Foundation of Foraminiferal Research. Retrieved from https://pubs.geoscienceworld.org/cushmanfoundation/books/book/2271/chapter-abstract/126275375

Westerhold, T., Marwan, N., Drury, A. J., Liebrand, D., Agnini, C., Anagnostou, E., et al. (2020). An astronomically dated record of Earth's climate and its predictability over the last 66 million years. *Science*, *369*(6509), 1383–1387. https://doi.org/10.1126/science.aba6853

Zachos, J. C., Dickens, G. R., & Zeebe, R. E. (2008). An early Cenozoic perspective on greenhouse warming and carbon-cycle dynamics. *Nature*, *451*(7176), 279–283. https://doi.org/10.1038/nature06588

Zachos, J. C., Pagani, M., Sloan, L., Thomas, E., & Billups, K. (2001). Trends, rhythms, and aberrations in global climate 65 Ma to present. *Science*, *292*(5517), 686–693. https://doi.org/10.1126/science.1059412

Zhang, Y. G., & Liu, X. (2018). Export depth of the TEX_{86} signal. *Paleoceanography and Paleoclimatology*, *33*(7), 666–671. https://doi.org/10.1029/2018PA003337

References From the Supporting Information

Meckler, A. N., Sexton, P. F., Piasecki, A. M., Leutert, T. J., Marquardt, J., Ziegler, M., et al. (2022). Cenozoic evolution of deep ocean temperature from clumped isotope thermometry. *Science*, *377*(6601), 86–90. https://doi.org/10.1126/science.abk0604

WOCE Hydrographic Programme, W. H. P. (2002). Hydrochemistry measured on water bottle samples during HUDSON cruise 18HU95003_1 on section AR13. *PANGAEA*. https://doi.org/10.1594/PANGAEA.837450